Old Dominion University
ODU Digital Commons

Summer 2001

Dynamical Sedimentary Models of Shallow Marine Environments

Yong Zhang
Old Dominion University

Follow this and additional works at: https://digitalcommons.odu.edu/oeas_etds

Part of the Geology Commons, and the Oceanography Commons

Recommended Citation

Zhang, Yong. "Dynamical Sedimentary Models of Shallow Marine Environments" (2001). Doctor of Philosophy (PhD), Dissertation, Ocean & Earth Sciences, Old Dominion University, DOI: 10.25777/e2cy-sd91
https://digitalcommons.odu.edu/oeas_etds/73

This Dissertation is brought to you for free and open access by the Ocean & Earth Sciences at ODU Digital Commons. It has been accepted for inclusion in OES Theses and Dissertations by an authorized administrator of ODU Digital Commons. For more information, please contact digitalcommons@odu.edu.

DYNAMICAL SEDIMENTARY MODELS OF SHALLOW MARINE ENVIRONMENTS

by

Yong Zhang

A Dissertation Submitted to the Faculty of Old Dominion University
in Partial Fulfillment of the Requirement for the Degree of

DOCTOR OF PHILOSOPHY

OCEANOGRAPHY

OLD DOMINION UNIVERSITY
August 2001

Approved by:

Donald J.P. Swift (Chair)

George F. Oertel (Member)

John M. Klinck (Member)

Alan W. Niedoroda (Member)

ABSTRACT

DYNAMICAL SEDIMENTARY MODELS OF SHALLOW MARINE ENVIRONMENTS

Yong Zhang
Old Dominion University, 2001
Director: Dr. Donald J. P. Swift

This treatise represents a contribution of quantitative, dynamical sedimentary modeling to the analytical understanding of sedimentary processes in shallow marine environments. The dynamical sedimentary models in this treatise numerically simulate the sedimentary processes from an event time scale, based on the fundamental physics of sediment dynamics in coastal and shelf depositional environments, to a longer, facies time scale. The simulated geologic processes serve to the illustrate shoreface equilibrium profile, shelf storm bed generation, and the shelf sedimentary facies system.

This treatise presents a nearshore profile evolution model for the abandoned Huanghe Delta, a two-dimensional storm deposition model, and a sedimentary facies model for the northern California continental shelf. These process-oriented geologic simulations are particularly well-suited for experimentation and sensitivity analysis because of their computational power. The dynamical sedimentary models support the progressive sorting and stratal condensation hypotheses for facies formation. The application of the models leads to significant geologic insights and dynamical understanding of the shallow marine sedimentary processes that traditional, descriptive sedimentology and stratigraphy are not able to provide.

This dissertation is dedicated to my wife, Keke, and my daughter, Julia.

Without their support and patience, this work would not look as good as you see now.

ACKNOWLEDGMENTS

I would like to deeply thank my advisor, Dr. Donald J.P Swift, for his continuous support, guidance and encouragement on my research presented in this dissertation. I would also like to thank my committee members, Drs. George F. Oertel, John M. Klinck and Alan W. Niedoroda for their kindly assistance and guidance.

I woud also like to thank the STRATFORM modelers, Drs. Chris Reed and Michael Steckler who provided generously assistance to my research. Special thanks should go to Cathy McConaugha for her long time logistics, finances and editing supports. I definitely owe a great thank you to Shejun Fan who deserves much more than I can express.

TABLE OF CONTENTS

Page

LIST OF TABLES vii

LIST OF FIGURES viii

Chapter

I. INTRODUCTION 1
  - GEOLOGIC PERSPECTIVE 1
  - PROBLEMS EXAMINED 2
    - The Equilibrium Profile on Muddy Coast 2
    - Storm Bed Generation on the Continental Shelf... 3
    - Sedimentary Facies on the Continental Shelf 5
  - APPROACH 8

II. MODELING OF THE COASTAL PROFILE EVOLUTION ON THE ABANDONED DELTA OF THE HUANGHE RIVER 12
  - INTRODUCTION 12
  - WAVE-INDUCED SHEAR STRESSES ON THE MUDDY PROFILE 14
  - WAVE-INDUCED EROSION RATES ON THE MUDDY PROFILE 25
    - Erosion Rate Equation 25
    - Solution of Erosion Rate Equation 26
    - Calculations 30
  - MUDDY PROFILE EVOLUTION 30
    - Expression of the Muddy Profile 30
    - The Effective Scouring Wave 33
    - Simulation 37
  - DISCUSSION 43
  - CONCLUSIONS 50

III. TWO-DIMENSIONAL NUMERICAL MODELING OF STORM DEPOSITION ON THE NORTHERN CALIFORNIA SHELF 52
  - INTRODUCTION 52
  - STORM-DEPOSITION MODEL 54
    - Conceptual Model 54

Chapter Page

Governing Equations 54
Algorithms for Important Processes of Storm-Bed Formation 58
Boundary Conditions 63
Current Field 68
Other Parameters 71
Numerical Solution 72
COMPUTATIONAL RESULTS 73
CONCLUSIONS 78

IV. SIMULATION OF SEDIMENTARY FACIES ON THE NORTHERN CALIFORNIA SHELF 81
INTRODUCTION 81
DYNAMICAL FACIES MODEL 85
General 85
Storm-Bed Formation 86
Storm-bed Succession Formation 87
Model Inputs 89
SIMULATION RESULTS 90
CONCLUSIONS 93

BIBLIOGRAPHY 96

VITA 113

LIST OF TABLES

Table Page

1. Erosion duration over the ebb period 29

LIST OF FIGURES

Figure Page

1. Location of the abandoned Huanghe River Delta ... 13

2. Coordinate system on a cross-shore section of muddy coast ... 16

3. Distribution of the surf zone similarity parameter $\xi_0 = \delta(H_b/L_0)^{-1/2}$, where H_b is the critical breaker height, L_0 is the deep wave length, and δ is the slope 17 ratio ... 17

4. Distribution of the maximum shear velocity in surf zone ... 20

5. Tidal gauge records in Lianyungang, the northern abandoned Huanghe Delta... 21

6. Variation of the shear velocity during ebb period ... 24

7. Distribution of the non-dimensional wave-induced erosion rates ... 31

8. Sedimentary features of Xiaodingang cross-section on the northern abandoned Huanghe Delta ... 35

9. Vertical variation of bulk density with depth in Lianyungang, the northern abandoned Huanghe Delta ... 36

10. Schematic drawing of the Effective Scouring Wave ... 39

11. Local wave climate (from the wave data at water depth of 8) ... 40

12. Cross-shore distribution of erosion rates ... 41

13. Evolution of nearshore muddy profiles on the northern abandoned Huanghe Delta ... 42

14. Location of field survey ... 44

Figure Page

15. Nearshore profile at Xiaodingang 45

16. Nearshore profile at Xiaowagang 48

17. Nearshore profile at Dalukou 49

18. Location of study area 53

19. A conceptual model of storm deposition on continental shelf 56

20. Measurements at101 cm above the sea floor in 60m water depth (VIMS S60) 70

21. (A) Storm-bed thickness as a function of current velocity, and (B) storm-bed thickness as a function of γ_0. 76

22. (A) Storm-bed thickness vs. critical shear stress for mud erosion, and (B) critical stress for mud deposition.. 77

23. Across-shelf variation of storm-bed thickness with respect to pre-storm Bottom sediment.. 79

24. Eel River sector of the Northern California Shelf, showing grain size gradients (Borgeld, 1985) 83

25. Facies template, configured for transgressive shelf setting..................... 84

26. Degree of stratal condensation for facies on the Northern California Shelf 91

27. Simulation vs. observation 92

CHAPTER I

INTRODUCTION

GEOLOGIC PERSPECTIVE

Extensive existence of shallow marine deposits in geologic records demonstrates the importance of coastal and shelf as sites of sediment deposition and accumulation. Rigorous sedimentation studies of modern shallow marine environment began in the early of last century (Johnston, 1919; Shepard, 1932; Emery, 1952). Various sedimentary facies models have been proposed to demonstrate the phenomena and processes of sedimentation (Curray, 1960, 1964; Swift, 1970, 1974) in modern shallow marine environment. The construction and use of morphological or facies models for the interpretation of sedimentary environments have been adopted by many geologists in recent years (Reading, 1986; Walker and James, 1992). However, these existing models are descriptive, searching for the processes that control facies and geometries by comparison of modern and ancient depositional environments, and interpreting sedimentary phenomena and processes by analogy and pattern-matching techniques. New methods for the analysis of shallow marine sedimentation are required that will provide a more systematic, quantitative, and analytic approach to the sedimentary deposits at successive temporal and spatial scales. Quantitative, dynamical modeling based on the fundamental physics of sediment dynamics is needed to simulate dynamical interaction of the sedimentary processes, and define the relevant responses of depositional systems.

The model journal for this dissertation is Marine Geology

This treatise contributes a suite of dynamical sedimentary models for the analysis of sedimentary processes in the shallow marine environment. Environments to which this treatise refers include coastal and shelf siliciclastic sedimentary environments. The numerical simulations represented here begin with the sedimentary processes at a single event time scale and are based on the fundamental physics of sediment transport in the depositional environment. They then are extended to the depositional responses at a longer, facies time scale. These process-oriented simulations are particularly well-suited for experimentation and sensitivity analysis because of their computational power. The dynamical sedimentary models lead to significant geologic insights and dynamical understandings of the shallow marine sedimentary processes that traditional, descriptive sedimentology and stratigraphy cannot easily provide or prove.

PROBLEMS EXAMINED

The Equilibrium Profile On Muddy Coast

It has been known since the turn of the last century that the nearshore profile is in some sense an equilibrium response to the hydraulic regime of nearshore waves (Fenneman, 1902; Johnson, 1919; Dietz, 1963; Moore and Curray, 1964; Dean, 1991; Horn, 1992; Roelvink and Broker, 1993; Niedoroda et al., 1995). An ideal nearshore profile takes the form of an exponential curve, concave upward, with the steeper inner segment being known as the shoreface, and the more gentle outer limb forming the inner shelf floor. However, most previous studies of coastal profile were conducted on sandy coasts. Few studies on the evolution of a muddy profile have been conducted. It has been recognized that muddy, or cohesive coasts are fundamentally different from sandy coasts in their sedimentary processes (Davidson-Arnott, 1986; Kamphuis, 1987; Yu et al., 1987; Zhang et al, 1989; Nairn and Southgate, 1993). On open cohesive coasts, the cohesive sediments on sea floor are resuspended into the water column by nearshore waves. The reworked cohesive sediments in suspension mode are dispersed far away by tidal currents owing to their very slow settling velocity, and are rarely redeposited in their original places. On the cohesive coasts of the Great Lakes, for instance, the coastal evolution is dominated by an irreversible erosion (Skafel and Bishop, 1994; Davidson-Arnott and Ollerhead, 1995).

Extensive muddy coasts exist in the delta depositional environment. Repeated river avulsion, leading to a cycle of growth and abandonment of successive deltas, is a characteristic of most delta systems. Large subdeltas form and are abandoned within 2000 years, whereas the small subdeltas exhibit life cycles of 200 years or less. A dynamical analysis of the equilibrium profile in the delta deposional environment and simulation of the steady-state geomorphic system will aid further understanding of the evolution of delta depositional systems, and therefore, the processes of continental margins.

Storm Bed Generation on the Continental Shelf

One of the important sedimentation modes in shelf depositional environment is event deposition during storms. On storm-dominated shelves, sedimentary textures and structures are constructed at the event scale, on the order of a few hours, or days duration. Storm sedimentation on continental shelves is mainly a response to wind-driven current and bottom oscillatory flow induced by surface water waves during storms (Swift et al., 1986; Duke et al., 1991). Depositional system on storm-dominated shelves are defined by their grain size, and the pattern of stratification (Seilacher, 1982). So far, few quantitative, dynamical studies of storm bed simulation have been conducted by applying the basic physics of sediment dynamics in response to storm-driven currents and wave oscillatory flows. The first attempt to simulate the formation of a storm bed succession was undertaken by Niedoroda et al. (1989). In this simulation, the storm bed formation is described by a 1-D sediment resuspension model in which the gradient of horizontal sediment flux is assumed to be zero. An arbitrary, time-averaged net sediment accumulation rate is introduced in order to simulate the preservation of beds. A prior time history of storm events, which is one realization of a stochastic storm wave climate, is used as input data for the model.

Thorne et al. (1991) modified the model of Niedoroda et al. (1989) by introducing the effect of sediment armoring to simulate the storm bed generation. The storm bed thickness is seen to have an empirical power function related to the storm return period. The coefficients in this relation are not mutually independent but vary simultaneously. Both models assume that the thickness of storm bed is always equal to the bottom sediment erosion depth, since the gradient of horizontal sediment flux is considered to be negligible during storms. Thus the net sediment accumulation, which is of most significance for bed preservation, is considered to be non-storm in origin. The reworking ratio, a parameter presenting the ratio of minimum bed thickness to the net sediment accumulation per storm event, is proposed to describe the degree of storm bed preservation (Thorne et al., 1991).

Strata formation on storm-dominated continental shelves is composed of two fundamental, episodic, sedimentary processes, i.e., storm bed generation and storm bed preservation. Storm beds are generated at water-sediment interface. Their formation is governed by the independent, time-variant, and random storm events characterized by such elements as storm type, intensity, location and trajectory, and by the bottom sediment-related boundary conditions caused by preceding storm event or by other factors (for example, river flooding).

Sedimentary Facies on the Continental Shelf

Few event deposits on continental shelves, however, can survive without modification. Most of each deposit will be resuspended and redeposited partly or totally by subsequent storms or other events. Only those event beds that have not been totally eroded are preserved as components in strata. Event bed preservation is very important in facies formation. The main factor governing the event bed preservation on continental shelves is net sediment accumulation (Nittrouer and Sternberg, 1981; Thorne et al., 1991). Observations of storm sedimentation on different modern continental shelves show that there is a significant amount of sediment transport occurring during storms in comparison with that during fair weather (Cacchione and Drake, 1982; Cacchione et al., 1987; Wright et al., 1986, 1991, 1994; Gross et al., 1992; Madsen et al., 1993; Green et al., 1995). Significant suspended sediment fluxes were observed during storms resulting in net (positive or negative) sediment accumulation. This net sediment accumulation, including that caused by bedload transport, is a key contribution to the preservation of beds. A storm acts not only as an agent for generation of a graded storm bed but also as a factor for preservation of preceding storm beds. A single storm can generate a bed. The extent to which this bed is preserved in the bed succession, however, depends completely on the discrete, random, net sediment accumulations generated by subsequent storm events. Thus, the results of an event bed generation model should include not only the formation of an event bed, but also the net sediment accumulation as an estimate of the contribution for preservation of preceding deposited beds. The storm-driven horizontal sediment flux should be formulated in modeling of facies formation on storm-dominated continental shelves in order to calculate the random sediment accumulation. In this case, a two-dimensional spatial frame is the minimum requirement for the process-related modeling of sedimentary facies.

The facies formation process is modeled as a dispersal system that relates input and output. On storm-dominated continental shelf, storms are certainly main inputs for this system. Because of the random nature of storms, this system is definitely a stochastic system, and its outputs, such as bed thickness, grain size, and net sediment accumulation, must also be stochastic variables. The random nature of the system restricts the simulation and prediction of real storm bed succession. When an event creates a bed on continental shelf, it will simultaneously destroy or modify previous deposited beds by erosion, particular during storms. As beds undergo burial, the degree to which they are preserved in bed succession depends not only on the intensity of the erosion, but also on the time series of events. For example, for any probability density distribution of storms (storm climate), there are many different realizations. Each realization can produce a unique bed succession. Thus, event bed preservation on continental margin behaves as a complicated, highly random process.

A depositional system has been defined as an assemblage of process-related facies (Fisher and McGowen, 1967). These facies, characterized by the differentiation of sedimentary textures and structures, are simultaneously deposited in a dispersal system (an assemblage of flow-linked depositional environments, see Swift et al., 1991). Facies differentiation on a modern storm-dominated continental shelf has been recognized by many authors (Kulm et al., 1975; Swift et al., 1978, Swift and Field, 1981; Aigner and Reineck, 1982; Allen, 1982). The concept of progressive sorting proposed by Russell (1939) has been used by Swift et al. (1972, 1991) to interpret the process that causes the cross-shelf differentiation of sedimentary texture on continental shelf. The deposited sediments are differentiated by grain size as sediment moves down a dispersal pathway during intermittent transport events, due to the higher probability of deposition of coarser grains. The energetic proximal environment will retain the coarser particles. The finer particles will be preferentially bypassed to the distal depositional environment. Thus, the grain size will vary systematically from proximal to distal environments. In addition to the progressive sorting, stratal condensation is also an important control of facies differentiation. The concept of stratal condensation, which can be defined as the ratio of preserved deposition to generated deposition, stems back to the concept of the completeness of sedimentary sequences proposed by Crowley (1984). In his numerical experiment, he thought that the preservation of sedimentary events acts as a low-pass filter to initial event beds. This low-pass filter gives rise to the temporal and spatial completeness of sedimentary sequences. The temporal completeness is defined as the ratio of the number of time lines preserved in a sedimentary sequence to the number of time lines generated during deposition. The spatial completeness is defined as the ratio of the thickness of sedimentary column to the total thickness of column generated during deposition. These concepts are proposed to present a quantitative measure on preservation process. Obviously, the cross-shelf variety of the strata condensation will result in the facies differentiation. Even though the progressive sorting and the stratal condensation are thought to be responsible for the formation of facies differentiation on continental margin, few attempts have been undertaken to test these hypotheses. These concepts are very difficult to test by field observation or application of traditional conceptual facies models due to lack of the power to simulate the dispersal system, i.e., the depositional environments in which the facies are formed.

APPROACH

This treatise presents three quantitative, dynamical sedimentary models for simulating and predicting sedimentation processes and sedimentary systems. Each of three models has been published in the open literature (Zhang et al., 1997, 1998, 1999).

The models are focused mainly on the problems described above. All these models are based on sediment dynamics, including both cohesive and non-cohesive sediments, on shallow marine environments. The abandoned delta of the Huanghe River in China is selected as one the study areas to deal with the problem of the equilibrium profile in a nearshore shallow marine setting. The northern California shelf is selected for the analysis of storm bed generation and sedimentary facies on storm-dominated continental shelf. The application of these models brings a new understanding and insight into sedimentary processes and sedimentary system responses in shallow marine environments, and the models serve to validate hypotheses that traditional facies models cannot adequately test.

Chapter II presents a quantitative, dynamical model for simulating and predicting the evolution of the nearshore muddy profile on the abandoned Huanghe Delta, which has been undergoing severe erosion since the shift of the Huanghe River in 1855. The model computes the wave-induced bed shear stresses on the muddy profile, and therefore calculates the erosion rate on surface cohesive sediments. The sea level fluctuation caused by the oceanic tide plays an important role in re-distributing the wave force and hence the sediment transport. This factor is introduced into the model. The steady-state nearshore muddy profile is simulated as a response to the average erosion rate of the local wave climate. However, at longer time scales, the averaged erosion rate is significantly influenced by the surface sand armoring and the vertical increase with depth of cohesive sediment consolidation during coastal erosion, leading to an irreversible evolution of the muddy profile. The *Effective Scouring Wave*, derived from local wave climate, is proposed to quantitatively incorporate these time-variant geological influences. The evolution of the muddy profile is determined by the change of the Effective Scouring Wave climate. The eroding muddy coast exhibits a monotonic, concave upward profile, whose curvature increases as the coastal erosion continues. The maximum curvature of the profile lies below the mean low tidal level. As the erosion continues, the maximum curvature moves down and shoreward. The position of the maximum curvature of the nearshore muddy profile can be used to estimate the evolutionary stages of the muddy coast. On the northern abandoned Huanghe Delta, the muddy profile approaches an equilibrium configuration when the maximum curvature reaches down to a water depth of about 6 m below the mean sea level. The model reveals a dynamical geomorphic system as a response to the abandonment on the Huanghe Delta. Similar patterns and evolutionary processes may be generalized to erosional muddy coasts in other shallow marine settings.

Chapter III presents a two-dimensional, across-shelf sediment transport model developed to simulate storm deposition on continental shelves. The structure of the model and related algorithms are discussed in detail. In the model, the time-dependent sediment resuspension, transportation and deposition, and across-shelf transport gradients are simulated as responses to storm waves on the Eel shelf, northern California. The simulations show that the pattern of storm deposition on the sandy inner shelf is different from that on the muddy middle and outer shelf. Storm bed thickness decreases seaward across the inshore sandy zone as far as the 50-m isobath. Farther seaward, storm bed thickness increases as the mud component in the sea floor increases, then decreases again, as the weakening of bottom wave motion with increasing depth becomes the dominant control. Storm bed thickness in the mud zone thus has a nearly symmetrical cross-shelf pattern, with the maximum thickness at a water depth of 70 m. The pattern suggests that while the sequence of new beds found in February of 1995 on the Eel shelf may have been flood-sourced, their geometry reflects storm resuspension and transport. The new muds found in these beds may have been reworked, transported and redeposited several times by storm waves and other oceanic forces.

Chapter IV represents a quantitative dynamical model developed to simulate the sedimentary facies on the northern California shelf. In the model, dispersal mechanisms at small time scales are described by deterministic sediment-transport equations. However, at large time scales, the shelf dispersal system is described in probabilistic terms owing to its stochastic behavior. The probability of storm-bed generation is described by the bed generation potential, P_g, which is determined by the probability density distribution function of the local storms. The bed preservation potential, P_p, valued between 0 and 1, is a parameter that describes the probable thickness of a storm bed that will be permanently buried in a bed succession. The extent of bed truncation depends on the extent of erosion and deposition caused by subsequent random storms. By estimating the preservation potentials of all generated storm beds, the most probable storm-bed succession is predicted. The computations support the hypothesis that sedimentary facies are produced by the coupled mechanisms of progressive sorting and stratal condensation on continental margins.

CHAPTER II

MODELING OF THE COASTAL PROFILE EVOLUTION ON THE ABANDONED DELTA OF THE HUANGHE RIVER

INTRODUCTION

The Huanghe River discharges an average of 1.1×10^9 tons of sediment into the sea annually (Qian and Dai, 1980), accounting for almost 10% of the fluvial sediments reaching oceans in the world. During AD 1128-1855, the Huanghe River flowed partly or exclusively into the Yellow Sea, forming a major delta in Jiangsu (Fig. 1). After 1855, when the Huanghe River shifted over the Shandong Peninsula and flowed into the Gulf of Bohai, the balance between the fluvial and the marine processes was modified significantly due to the sudden loss of the Huanghe sediment discharge. Consequently, the abandoned delta, composed mainly of silt and clay with a mean grain size of 7-8 ϕ, has been undergoing severe erosion since then.

This chapter presents a dynamical model designed to simulate and predict the evolution of the nearshore muddy profile on the northern abandoned Huanghe Delta. Shoaling waves are one of the most important factors causing erosion on muddy coasts, particularly on the open coasts of abandoned deltas (Coleman, 1988). In the model, the

-induced bottom shear stresses on the muddy profile, and hence the erosion rate of

is calculated. One of the important mechanisms in governing nearshore

s on muddy coasts is the periodic shift of surf zone due to the sea

y tide. It is of considerable importance in determining the cross-shore

wave force and hence the sediment transport. The sea level fluctuation is

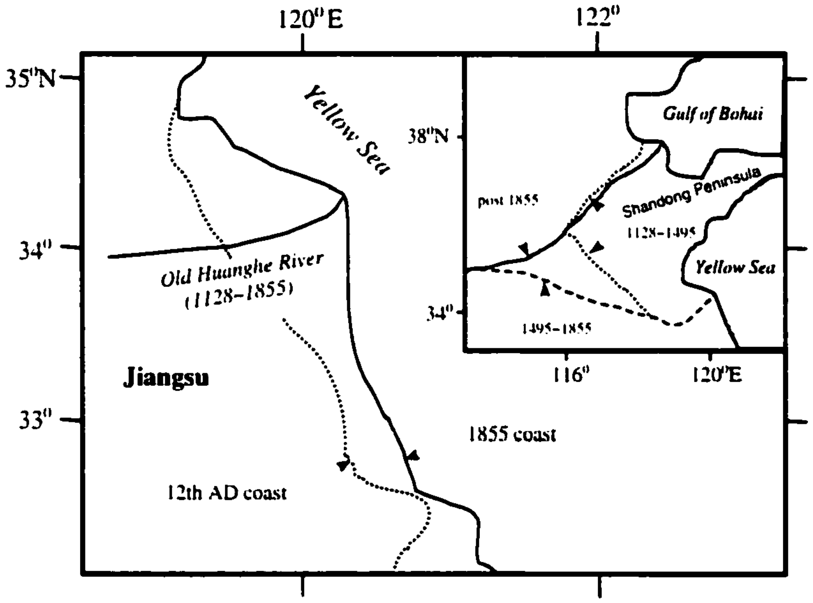
120°E
122°
35°N
34°
33°
Yellow Sea
Old Huanghe River (1128-1855)
Jiangsu
12th AD coast
1855 coast
38°N
34°
116°
120°E
Gulf of Bohai
post 1855
Shandong Peninsula
1128-1495
Yellow Sea
1495-1855

Fig. 1. Location of the abandoned Huanghe River Delta.

therefore introduced into the model. The steady-state muddy profile is simulated as a response to the average erosion rate of the local wave climate. This average erosion rate, at long-time scales, is significantly influenced by the surface sand armoring and the vertical increase with depth of cohesive sediment consolidation. The concept of the *Effective Scouring Wave* is proposed to numerically incorporate these influences. The evolution of the muddy profiles, therefore, is simulated by the model with respect to the variation of the Effective Scouring Wave climate. The model is used to predict the stability of the muddy profiles and the trend of the coastal erosion in the northern abandoned Huanghe Delta.

WAVE-INDUCED SHEAR STRESSES ON THE MUDDY PROFILE

A two-dimensional coordinate system on a cross-shore section of a plane profile is defined for the purpose of this study (Fig. 2). The erosive force on a cohesive bed is usually characterized by flow-induced bed shear stress. The erosion rate of cohesive bed is expressed as a function of the excess shear stress τ - τ_c (Mehta et al., 1989; Teisson et al., 1993), where τ is the bed shear stress and τ_c is the critical shear stress for erosion. The surf zone is the area with the most intense sediment transport because of the high intensity of turbulence caused by wave breaking (Fredsoe and Deigaard, 1992). In surf zone, the turbulent kinetic energy of broken waves is produced in the surface roller as well as in the wave boundary layer at bottom (Battjes and Sakai, 1981; Basco, 1985; Deigaard et al., 1986). The energy loss due to wave breaking is much larger than that caused by the dissipation in bottom boundary layer (Svendsen, 1987). Eddy diffusivity is therefore much larger outside the wave boundary layer, so that more sediments can be carried in suspension away from bed. A stepwise regression analysis of the relationship between the suspended sediment concentration and the simultaneously measured nearshore hydrodynamic regime (wave height, wave direction, tidal range, etc.) indicates that the breaking and broken waves are dominant forces controlling the sediment suspension on the northern abandoned Huanghe Delta (Zhang et al., 1989).

The occurrence of different types of breaking waves depends on the steepness of incoming wave and nearshore slope. The surf zone similarity parameter, ξ_0, proposed by Battjes (1974), is used here to identify the types of breaking waves in the study area. ξ_0 is calculated with respect to the incident wave height and the slope ratio based on the local average wave period of 3.0 s in the study area (from the observation data of 1961-1973 at the Lianyungang Ocean Observation Station). Fig. 3 demonstrates the results of the calculation. The subaquatic slope of a muddy coast is usually very gentle. In the northern abandoned Huanghe Delta, the nearshore slopes vary from 0.002 to 0.0005. A spilling-dominant situation occurs when ξ_0 is less than 0.4 - 0.5 (Battjes, 1974). Fig. 3 indicates that ξ_0 is far less than that threshold, so spilling is the dominant breaking wave type in this area.

The turbulence of spilling is mainly caused by surface roller vortex (Peregrine and Svendsen, 1978; Basco, 1985; Deigaard et al., 1986). As spilling propagates toward shore, the turbulence extends down to sea floor. The fluid field caused by spilling exhibits a quasi-stable state (Peregrine and Svendsen, 1978). Because of the flatness of muddy profile, breaking waves are usually transformed into bore-like broken waves in extensive inner surf zone. The height of these periodic broken waves decays gradually in surf zone. The linear wave theory has been widely used in the surf zone hydrodynamics.

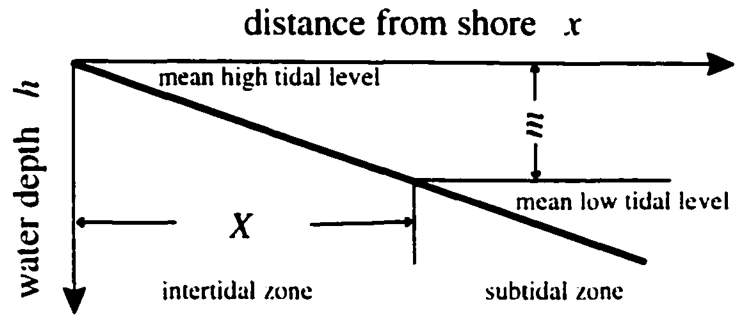
distance from shore x
water depth h
mean high tidal level
m
mean low tidal level
X
intertidal zone
subtidal zone

Fig. 2. Coordinate system on a cross-shore section of muddy coast.

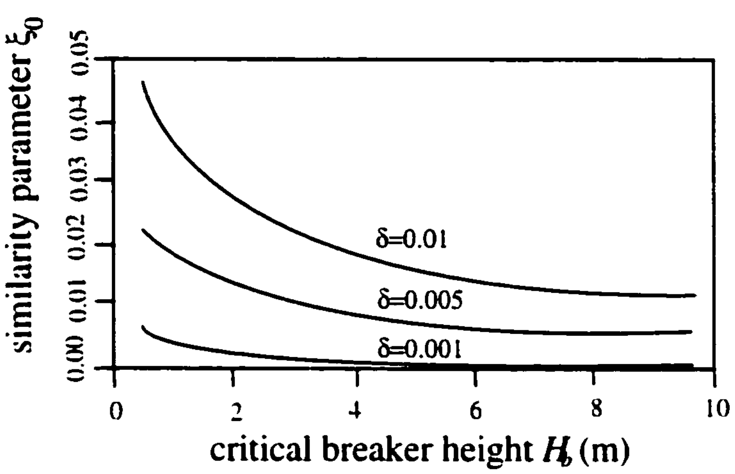

Fig. 3. Distribution of the surf zone similarity parameter $\xi_0 = \delta(H_b/L_0)^{-1/2}$, where H_b is the critical breaker height, L_0 is the deep wave length, and δ is the slope ratio.

for example, the wave energy transformation, under the spilling condition (Battjes and Janssen, 1978; Thornton and Guza, 1983; Lippmann et al., 1996). Recently, Cox et al. (1996) found that the bottom shear stress caused by a spilling could be fairly well estimated by the linear wave theory. In the model, the broken waves are described by the linear wave theory as a first order approximation for estimating the wave-induced bed shear stress on the nearshore surface. The shear stress field over the entire surf zone is obtained by extending this assumption into the outer surf zone, based on the consideration that there is little difference for turbulence transport of a spilling between inner and outer surf zone (Ting and Kirby, 1996).

The wave height decay of spilling in a plane sea floor can be estimated by assuming that the wave energy becomes saturated everywhere within surf zone so that local wave height H is a linear function of local water depth h (Thornton and Guza, 1982), i.e., $H/h = \gamma$, where γ is the breaker index. From their field measurements, Sallenger and Holman (1985) found that the γ is not constant but varies between 0.29 to 0.55. Based on the nearshore wave observations in Lianyungang of the northern abandoned Huanghe Delta, Jin and Zhang (1983) have established an empirical equation to estimate the wave height decay in the surf zone with respect to the critical breaker water depth and the local water depth:

$$H^{2.5} = 0.45h_b^{1.5} - 0.35h_b^{-0.1}(h_b^{2.6} - h^{2.6}) \qquad (1)$$

where H is the one-tenth mean wave height in the surf zone, h_b is the critical breaker water depth, and h is the water depth. The maximum bed shear stress during a wave period is expressed as $\tau = 0.5\rho f_w u_b^2$ (Jonsson, 1966). Here, ρ is the water density, f_w is the wave friction factor, and u_b is the maximum wave orbital velocity near bottom. So, the maximum bed shear stress expressed in terms of shear velocity is:

$$u_{*m} = \sqrt{\frac{f_w}{2}} u_b = \sqrt{\frac{f_w}{2}} \frac{\pi H}{T sh(kh)} \quad (2)$$

where u_{*m} is the maximum shear velocity, T is the wave period and k is the wave number. Substituting Eq. 1 into Eq. 2 yields the cross-shore distribution of the maximum shear velocities in the surf zone with respect to various incident wave heights (Fig. 4).

One of the important mechanisms in governing the nearshore hydrodynamic processes on muddy coasts is the periodic cross-shore shift of the surf zone due to tidal sea level fluctuation. It is of considerable importance in determining the cross-shore distribution of the wave forces and hence the sediment transport on the muddy coasts of the abandoned Huanghe Delta. There are extensive tidal flats as a consequence of the very gentle nearshore slopes. For instance, with an average local tidal range of 3.2 m and a nearshore slope of 0.001, sea level change during the half period of the local semidiurnal tide (6.2 hr) may result in a cross-shore surf zone shift of 3,200 m, leading to a significant time-variant redistribution of the wave-induced bed shear stress. As a result, the bed shear stress exhibits the character of complicated time-dependence, which is a simultaneous response to the random incident waves and to the periodic tidal sea level fluctuation. The field data show that the sea level changes in the tidal cycles present an almost symmetric sinusoidal curve in the study area (Fig. 5). Thus, the variation of the sea level can be expressed by a sinusoidal function. Therefore, the change of water depth h at an offshore distance x during ebb period is described by:

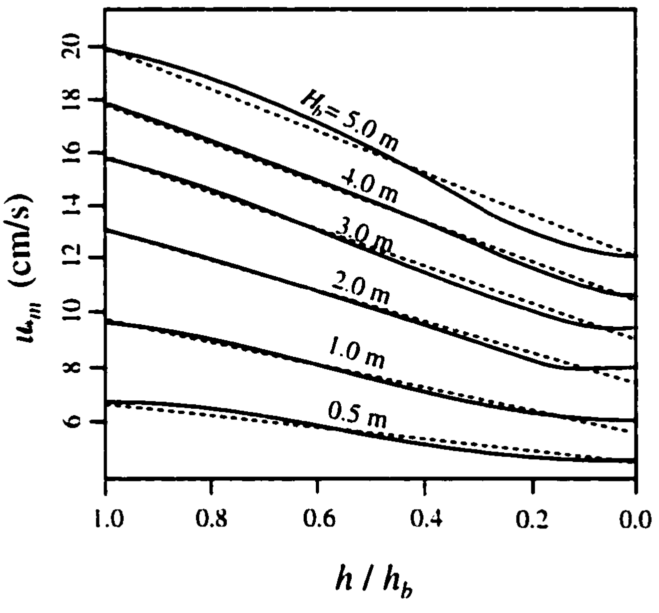

Fig. 4. Distribution of the maximum shear velocity in surf zone. The solid lines are calculated from Eq. 2, and dotted lines are calculated from Eq. 4.

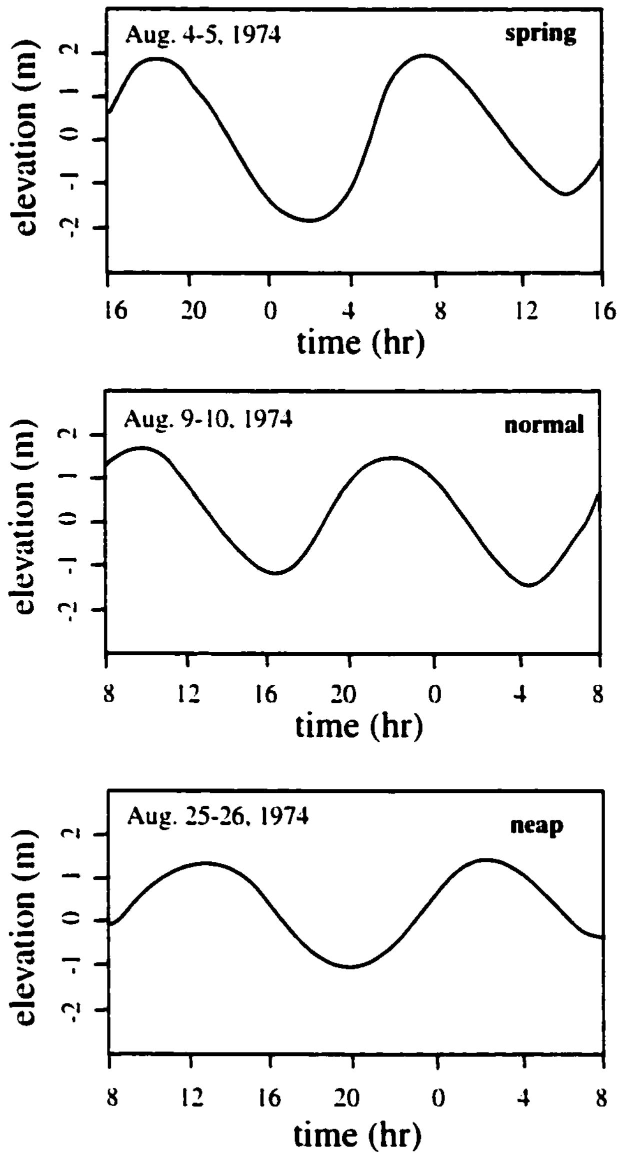

Fig. 5. Tidal gauge records in Lianyungang, the northern abandoned Huanghe Delta.

$$h = \frac{m}{2}\left(\cos\frac{\pi t}{T_e} - 1\right) + x\delta \tag{3}$$

where T_e is the ebb period, m is the mean tidal range, δ is the slope ratio and x is the offshore distance defined in Fig. 2.

The maximum shear velocity of broken waves shows a nearly linear decay in the surf zone (Fig. 4) so that its cross-shore variation can be approximated by a linear function. The decay parameter K' with respect to the incident wave height, H_b, is obtained through best-fitting on the linearized maximum shear velocity curves in Fig. 4, with the result that:

$$K' = -(0.0022 + 0.015H_b)$$

So, the maximum shear velocity in the surf zone is expressed by:

$$u_{*m} = \sqrt{\frac{f_w}{2}}\frac{\pi H_b}{Tsh(kh_b)} + K'(1 - \frac{h}{h_b}) \tag{4}$$

Substituting Eq. 3 into Eq. 4, the maximum shear velocity during semi-tidal cycle, for a given incident wave height, is:

$$u_{*m} = A + B\eta \tag{5}$$

where:

$$A = \sqrt{\frac{f_w}{2}}\frac{\pi H_b}{Tsh(kh_b)} + K'$$

$$B = -K'\frac{m}{2h_b}$$

$$\eta = \cos\left(\frac{\pi t}{T_e}\right) + \frac{2x}{X} - 1$$

where X is the width of intertidal zone (Fig. 2). The term A represents the maximum shear velocity at the shoreline, at the time of high tide. The term η varies with time and distance from shore. By using the average wave period $T = 3.0$ s, the mean tidal range $m = 3.2$ m, the local semi-tidal period $T_e = 6.2$ hr, the time-dependent maximum shear velocity is calculated by Eq. 5. The results are plotted in Fig. 6. As the incident wave height increases, the width of the surf zone increases as well as the intensity of the bed shear stress. As the sea level falls during ebb, the surf zone shifts seaward so that the intertidal zone is gradually exposed to air. For a given incident wave height, any location in the cross-shore profile undergoes a monotonic decrease of the bed shear stress with time during ebb as long as the surf zone passes on it (Fig. 6). For flood tide, however, the reverse is true. The time series of bed shear stresses is characterized by variation in space. For instance, at the time of high tide ($t = 0$), the middle of the intertidal zone ($x/X = 0.5$) is located outside the surf zone when the incident wave heights are less than 1.2 m so that no breaker erosion occurs. Whereas it will lie inside the surf zones when the incident wave heights are larger than 1.2 m. In this case, the erosion could start at the very beginning of the ebb cycle. As the tide falls, the bed shear stress at the middle of intertidal zone, unlike that at the permanent submerged subtidal zone, will cease immediately at the time of $T_e/2$ owing to subaerial exposure. It can be concluded that the cross-shore bed shear stress is closely associated with the offshore distance, the tidal cycle and the random variation of incident wave heights.

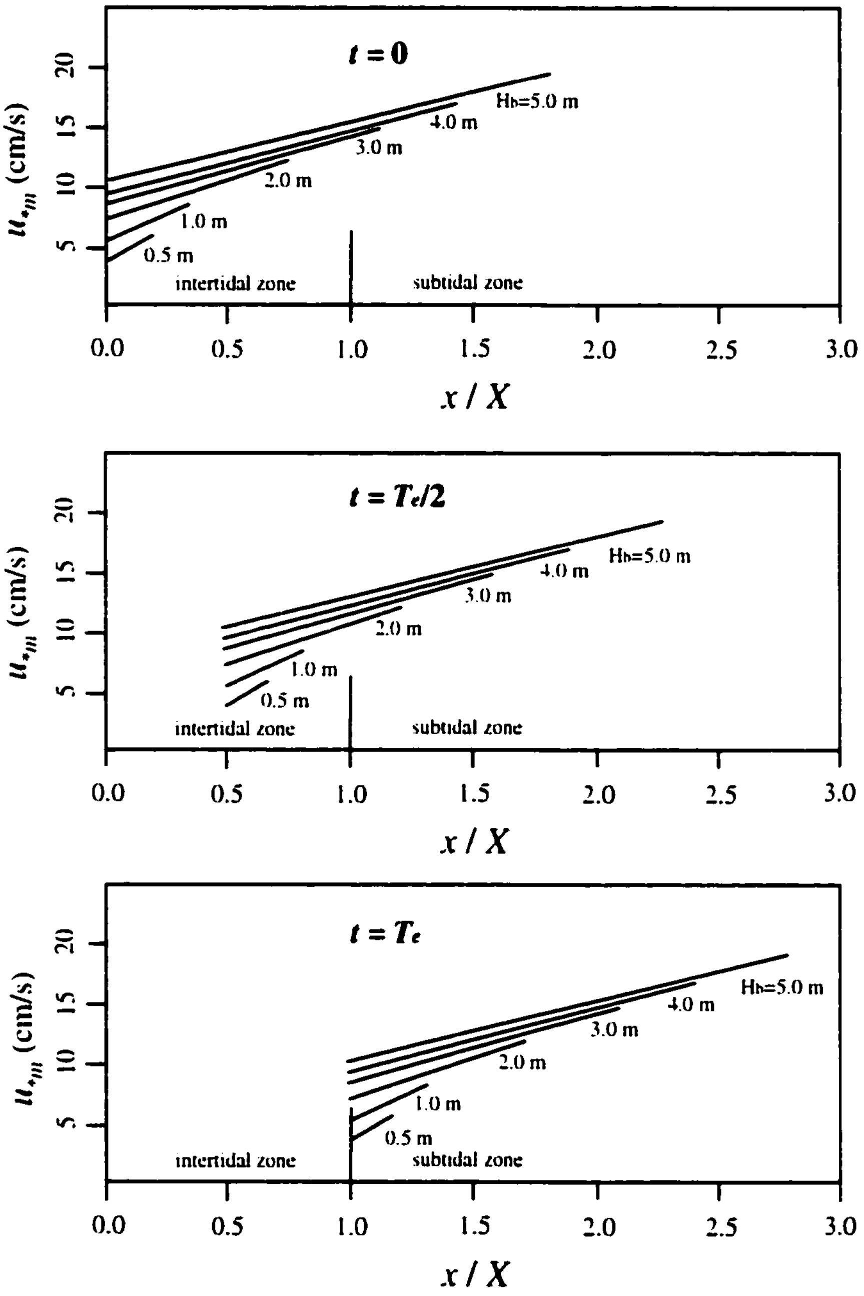

Fig. 6. Variation of the shear velocity during ebb period.

WAVE-INDUCED EROSION RATES ON THE MUDDY PROFILE

Erosion Rate Equation

The erosion rate on a cohesive bed is generally expressed empirically in terms of the excess shear stress (Mehta et al., 1989; Teisson et al., 1993). The equation of erosion rate proposed by Partheniades (1965) has been widely used in the modeling of cohesive sediment transport (Ariathurai and Krone, 1976; Ariathurai and Arulanandan, 1978; Nicholson and O'Connor, 1986; Mehta et al., 1989):

$$\frac{dE}{dt} = M\left\{\left(\frac{u_*}{u_{*c}}\right)^2 - 1\right\} \qquad u_* \geq u_{*c}$$

$$\frac{dE}{dt} = 0 \qquad u_* < u_{*c} \tag{6}$$

where E is the mass of eroded cohesive sediments per unit area (kg/m^2), M is the erosion coefficient (kg/m^{2}s) that is closely related to the physico-chemical properties of cohesive sediment, u_* and u_{*c} are the shear velocity and the critical shear velocity for erosion respectively.

The bed shear stress varies periodically due to the oscillatory flow of waves. Using u_{*m} as the wave-period-averaged bed shear stress, Eq. 6 is integrated over a wave period. This yields:

$$E = M\left\{\left(\frac{u_{*m}}{u_{*c}}\right)^2 - 1\right\}\Delta t$$

where Δt is the duration of the excess shear stress within a wave period. Introducing $(1-u_{*c}/u_{*m})T$ as an approximation of Δt yields:

$$E = M\left\{\left(\frac{u_{*m}}{u_{*c}}\right)^2 - 1\right\}\left(1 - \frac{u_{*c}}{u_{*m}}\right)T$$

Thus, the wave-period-averaged erosion rate on a cohesive bed is:

$$E = M\left\{\left(\frac{u_{*m}}{u_{*c}}\right)^2 - 1\right\}\left(1 - \frac{u_{*c}}{u_{*m}}\right) \tag{7}$$

The total amount of resuspended cohesive sediments during a semi-tidal cycle is:

$$E = \int_{\alpha}^{\beta} M\left\{\left(\frac{u_{*m}}{u_{*c}}\right)^2 - 1\right\}\left(1 - \frac{u_{*c}}{u_{*m}}\right)dt \tag{8}$$

where α and β represent the starting time and the ending time of erosion during an ebb cycle respectively. They are associated with the incident wave height H_b, the offshore distance x, and the critical shear velocity u_{*c}. Eq. 8 predicts the cross-shore variation of the time-variant erosion rates on a wave-dominated muddy coast under the conditions of tidal sea-level fluctuation. The value of u_{*m} is given by Eq. 5.

Solution of Erosion Rate Equation

Beginning time of erosion α

Water depth h_x, at location x at the time of high tide, is defined by $h_x = x\delta$. For a given incident wave height, if x is located inside surf zone, erosion may occur at the beginning of ebb, whereas if it is located outside surf zone, erosion may only occur at the time when surf zone passes over it. Obviously, for the area where the water depth, h_x, is greater than $h_b + m$, the surf zone cannot reach that area even at the time of low tide. By Eq. 3, the beginning time of erosion α is determined as:

$$\alpha = \frac{T_e}{\pi}\cos^{-1}\left\{1 - \frac{2}{m}\left(x\delta - h_b\right)\right\} \qquad h_b < h_x < h_b + m$$

$$\alpha = 0 \qquad h_x \le h_b \tag{9}$$

Ending time of erosion β

The ending time of erosion β is mainly controlled by the excess shear velocity u_{*m}-u_{*c}. Erosion will cease as soon as $u_{*m} \le u_{*c}$. During an ebb, u_{*m} decreases owing to the seaward movement of surf zone (Fig. 6). Eq. 5 of u_{*m} can be rewritten as follows:

$$u_{*m} = a + bc \tag{10}$$

where:

$$a = \sqrt{\frac{f_w}{2}}\frac{\pi H_b}{Tsh(kh_b)} + K'(1 - \frac{x\delta}{h_b}) - b$$

$$b = -\frac{K'm}{2h_b}$$

$$c = \cos\left(\frac{\pi t}{T_e}\right)$$

The shear velocity has a maximum value, $u_{*max} = a+b$, when $c = 1$ at the beginning time of $t = 0$. Then, it decreases as c decreases with time. The minimum value of shear velocity, u_{*min}, however, is dependent on the submergence time t_x. In subtidal zone (Fig. 2), $t_x = T_e$ so that u_{*min} equals to a-b since $c = -1$. Nevertheless, in intertidal zone, t_x is less than T_e due to subaerial exposure. The value of u_{*min} is thus between $a+b$ and $a-b$ since $|c| < 1$. So, if μ is denoted as $-c(t_x)$, u_{*min} can be expressed as a-μb. Obviously, no erosion will occur when $u_{*c} > u_{*max}$. If $u_{*c} \le a$-μb, the erosion will proceed until the ending time of ebb t_x. If $a-\mu b < u_{\bullet c} < a+b$, there must be a time during ebb at which $u_{\bullet m}$ equals to $u_{\bullet c}$, implying the ending time of erosion. Therefore, β is determined as:

$$
\begin{aligned}
&\beta = 0 && u_{\bullet c} \geq a+b \\
&\beta = \frac{T_e}{\pi}\cos^{-1}\left(\frac{u_{\bullet c}-a}{b}\right) && a-\mu b < u_{\bullet c} > a+b \qquad (11) \\
&\beta = t_x && u_{\bullet c} \leq a-\mu b
\end{aligned}
$$

Analytical solution

Under the conditions of $u_{\bullet c} < u_{\bullet max}$, the erosion duration can be grouped into four possible classes shown in Table 1. Integrating Eq. 8 between limits with respect to four classes yields:

$$
E = \begin{cases} E_1 & 1 \\ E_2 & 2 \\ E_1 - E_3 & 3 \\ E_2 - E_3 & 4 \end{cases}
$$

where:

$$
E_1 = MT\left\{\left(\frac{a^2 - au_{\bullet c} - u_{\bullet c}^2}{u_{\bullet c}^2}\right) + \frac{b^2}{2u_{\bullet c}} + \frac{u_{\bullet c}}{\sqrt{a^2-b^2}}\right\}
$$

$$
\begin{aligned}
E_2 = \frac{MT}{\pi}\Bigg\{&\left(\frac{2(a^2 - au_{\bullet c} - u_{\bullet c}^2)+b^2}{2u_{\bullet c}}\right)\cos^{-1}N + \left(\frac{Nb^2 - 4ab - 2bu_{\bullet c}}{2u_{\bullet c}}\right)\sqrt{1-N^2} \\
&+ \frac{2u_{\bullet c}}{\sqrt{a^2-b^2}}\,arctg\left(\frac{(a-b)\sqrt{1-N^2}}{(1+N)\sqrt{a^2-b^2}}\right)\Bigg\}
\end{aligned}
$$

where $N = (u_{\bullet c}-a)/b$. E_3 is identical with E_2 except that the N is displaced by $D = 1\text{-}2(x\delta\text{-}h_b)/m$.

Table 1

Erosion duration over ebb period

	α	β
1	0	t_x
2	0	$\frac{T_e}{\pi}\cos^{-1}\left(\frac{u_{*c}-a}{b}\right)$
3	$\frac{T_e}{\pi}\cos^{-1}\left\{1-\frac{2}{m}\left(x\delta-h_b\right)\right\}$	t_x
4	$\frac{T_e}{\pi}\cos^{-1}\left\{1-\frac{2}{m}\left(x\delta-h_b\right)\right\}$	$\frac{T_e}{\pi}\cos^{-1}\left(\frac{u_{*c}-a}{b}\right)$

Calculations

The critical shear velocity for erosion, u_{*c}, is generally determined through field measurements or laboratory experiments (Ariathurai and Arulanandan, 1978; Parchure and Mehta, 1985; Gu et al., 1990; Mimura, 1993; Schunemann and Kuhl, 1993). In the flume experiments on the muds of Lianyungang at the northern abandoned Huanghe Delta, Huang and Sun (1985) found that u_{*c} varies from 0.49 cm/s to 5.33 cm/s as the bulk density of the mud increases from 1.05 to 1.50 g/cm^3. For the local T_e = 6.2 hr and m = 3.2 m, the across-shore distribution of erosion rates with respect to the incident wave height and the critical shear velocity are calculated by Eq. 8. The results are shown in Fig. 7, which lead to the conclusions that, 1) as the incident wave height increases, the erosion rate increases, the horizontal scale of erosion expands, and the position of maximum erosion rate moves seaward; 2) the discrepancy of the erosion rates between different incident waves increases seaward, and 3) the erosion rate decreases significantly as the resistance of the mud to erosion increases. When u_{*c} reaches 5 cm/s, the erosion is negligible for the incident wave heights of less than 1 m. This result confirms that the erosion of a well-consolidated muddy coast, for example, that of an abandoned delta, is probably caused by stronger waves during storms.

MUDDY PROFILE EVOLUTION

Expression of the Muddy Profile

On an abandoned delta, erosion processes govern the evolution of coast. At the northern abandoned Huanghe Delta, the coast is composed mainly of silt and clay with a mean grain size of 7-8 ϕ. The bottom cohesive sediments are resuspended by the

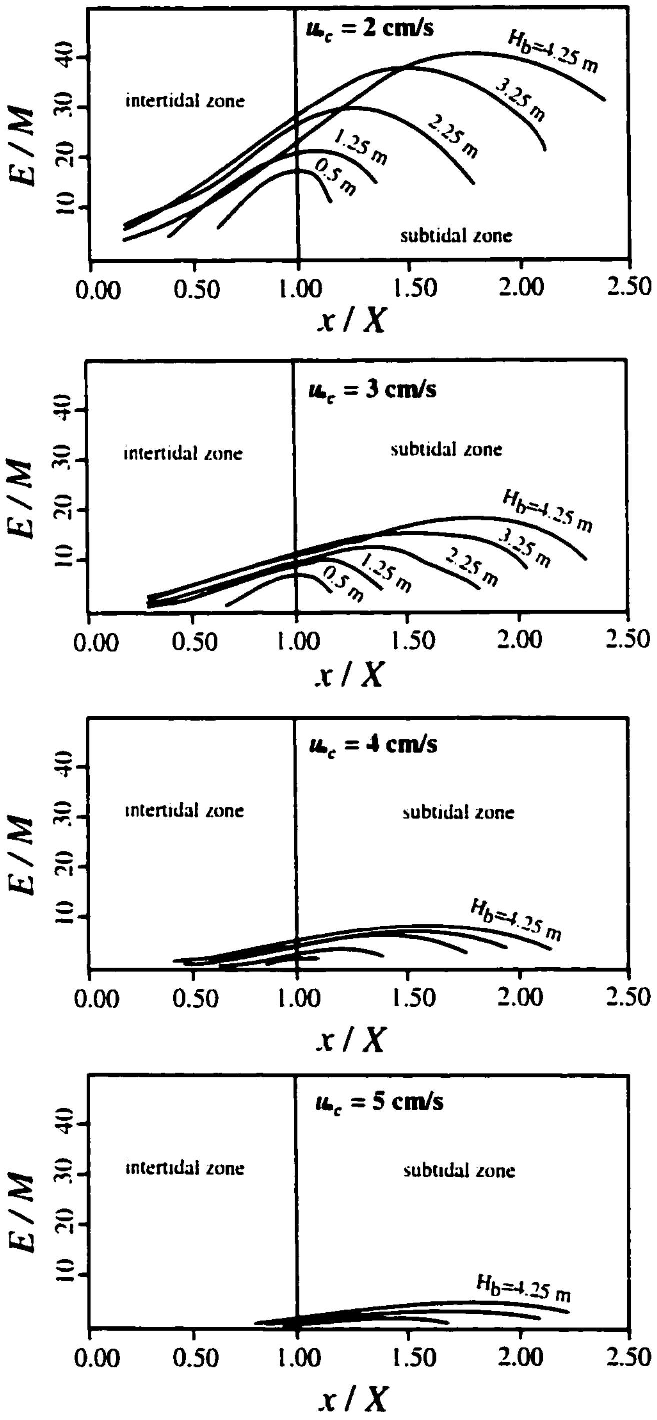

Fig. 7. Distribution of the non-dimensional wave-induced erosion rates.

nearshore breaking or broken waves, and are mainly dispersed away by the tidal currents in a suspension mode. Like the till coasts in the Great Lakes (Kamphuis, 1987), the eroded sediments are rarely redeposited in their original places, and the evolution of the muddy profile is dominated by an irreversible erosion (Yu et al., 1987). Therefore, in the model, the local redeposition of eroded sediments is disregarded and the coastal profile is considered to be fully determined by the cross-shore distribution of erosion rates. The erosion rate E is characterized by a random variation because the bed shear stress is a random variable associated with a stochastic wave regime. The state of a muddy profile over a certain time scale is actually determined by a randomly varying wave series, rather than by a single wave class. Pilkey et al. (1993) pointed out that a stable nearshore profile is virtually controlled by wave climate in a given geological setting. For the cohesive coasts of the Great Lakes, Davidson-Arnott and Ollerhead (1995) also found that the muddy profile is determined by the cumulative wave energy. In this study, a steady-state muddy profile is considered to be controlled by the wave climate. Its pattern is determined by the average erosion rate E_m of the wave climate. E_m can be quantitatively described by the expected value of E with respect to a wave climate as:

$$E_m = \int_0^\infty E(H_b)P(H_b)dH_b \qquad (12)$$

where $E(H_b)$ is the erosion rate of an individual wave class given by Eq. 8, $P(H_b)$ is the probability density function of the local waves just outside surf zone. Eq. 12 describes the cross-shore distribution of the mean erosion rate for a given wave climate, by which the shape of a steady-state muddy profile is determined.

The Effective Scouring Wave

It has been recognized that muddy coasts are fundamentally different from sandy coasts in their coastal processes (Davidson-Arnott, 1986; Kamphuis, 1987; Yu et al., 1987; Zhang et al., 1989; Nairn and Southgate, 1993). An erosional muddy profile is a response to a nearshore wave climate, rather than a single wave. However, not all waves can cause erosion. Fig. 7 illustrates that the critical shear velocity for erosion, u_{*c}, plays an important role in controlling the erosion of mud. On a muddy coast, u_{*c} is a time-dependent variable. It is closely related to the physico-chemical properties of cohesive bed that vary as coastal erosion proceeds. There are two fundamental geological processes that are mainly responsible for the variation of u_{*c} during long-term muddy coastal erosion. In the first, the surface of mud bed becomes armored owing to wave winnowing as coastal erosion proceeds. Cohesive sediments are reworked by waves into sea water and then are dispersed away from nearshore zone by tidal currents. Nevertheless, coarse particles such as sands and biological debris will redeposit locally owing to their high settling velocities so that a coarse sediment layer is gradually formed over the mud bed. An overlying coarse sediment layer of 10-15 cm thick has been found in the intertidal zone of our study area (Fig. 8). The coarse layer becomes more resistant to erosion with time because it thickens as the coastal erosion proceeds. Thus the erosion can not reach down into the cohesive bed unless the whole coarse layer overlying it is being reworked. Only stronger waves can rework the whole sand layer and scour down into the cohesive bed below it. An intermittent thin sand and gravel layer overlying a cohesive bottom was also found on the glacial till coasts of the Great Lakes (Kamphuis, 1987). The protective effect of this coarse layer on the cohesive sediments below it has been studied by Kamphuis (1990), Bishop et al. (1992), and Skafel and Bishop (1994). Through the flume experiments, Kamphuis (1990) concluded that if the surface granular material can be eroded, the cohesive sediments below it will also be eroded. If the granular material is stable, the cohesive sediments will not be eroded.

Secondly, as coastal erosion proceeds, the older muds that were deposited during the early stage of delta progradation, are progressively exposed to sea water. The farther the coast retreats and the deeper the shoreface downcuts, the older the exposed muds will be. Older muds usually have a higher resistance to erosion because of the longer time of consolidation. Fig. 9 shows a vertical increasing distribution with depth of the bulk density in our study area. Similar distributions were found at the tidal flats of the Wadden Sea (Schunemann and Kuhl, 1993). The bulk density of cohesive sediment is one of the most important parameters controlling the critical shear stress of erosion (Migniot, 1968; Mehta et al., 1989). A higher bulk density of cohesive bed results in a higher critical bed shear stress for erosion, leading to a lower erosion rate. The vertical increased bulk density with depth in our study area will result in the decrease of the erosion rate with time.

Therefore, at long-time scales, the range of waves that are able to cause erosion decreases with the change of sedimentary structure on sea floor. The erosion induced by small waves will cease as the profile evolves, and the muddy profile is progressively governed by higher waves. We define the wave that is capable of generating erosion on muddy substrate as the *Effective Scouring Wave*. Its height is expressed as H_e. Effective Scouring Waves in a given area consist of a frequency band within the spectrum of local

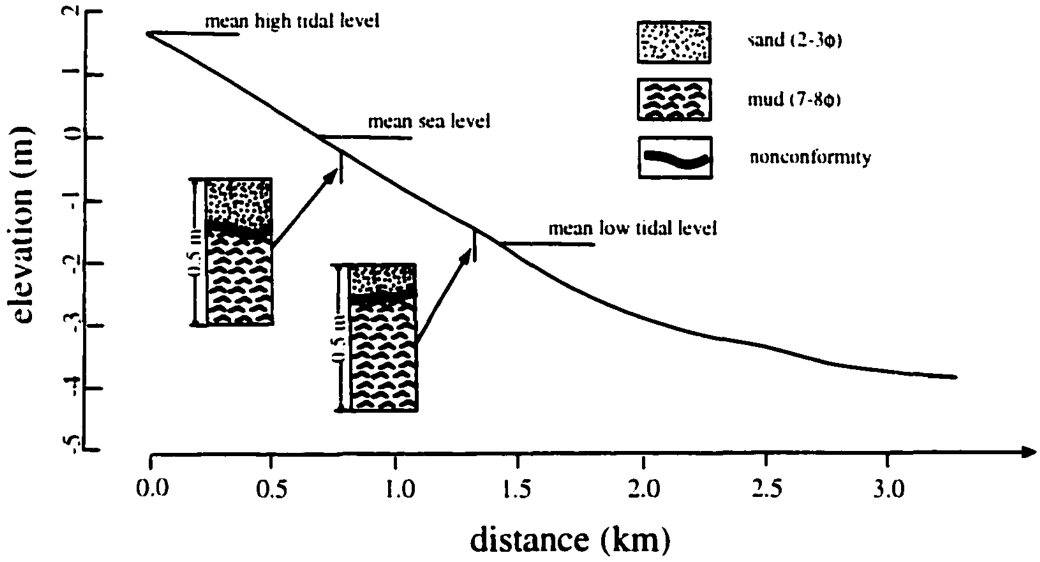

Fig. 8. Sedimentary features of Xiaodingang cross-section on the northern abandoned Huanghe Delta.

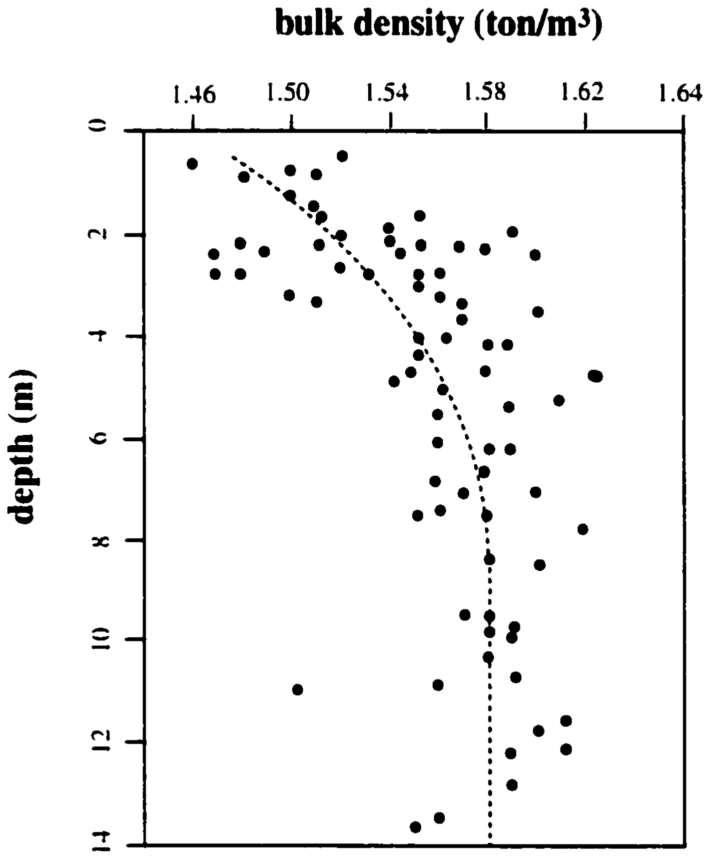

Fig. 9. Vertical variation of bulk density with depth in Lianyungang, the northern abandoned Huanghe Delta.

waves, from a minimum value $H_{e,min}$ that increases with time as the coastal erosion proceeds, to a maximum value of $H_{e,max}$ that is the maximum wave height in local wave climate during the period of concern. The muddy profile of Eq. 12 is thus rewritten in terms of the Effective Scouring Wave as:

$$E_m = \int_{H_{e,min}}^{H_{e,max}} E(H_e)P_e(H_e)dH_e \tag{13}$$

where $P_e(H_e)$ is the probability density function of Effective Scouring Wave. Substituting Eq. 8 into Eq. 13 and considering the symmetry of the tidal cycles (Fig. 5), a steady-state, wave-climate-averaged muddy profile, therefore, can be described by:

$$E_m = 2M \int_{H_{e,min}}^{H_{e,max}} \int_{\alpha}^{\beta} \left\{ \left(\frac{u_{*m}}{u_{*c}} \right)^2 - 1 \right\} \left(1 - \frac{u_{*c}}{u_{*m}} \right) P_e(H_e) dt dH_e \tag{14}$$

Simulation

The time-variant $H_{e,min}$ determines the variation of the Effective Scouring Wave climate. However, it is hard to be estimated because of the lack of quantitative knowledge of the mechanics behind the geological processes that affect it. In this study, $H_{e,min}$ is assumed to be a discrete, linear function with time, shifting from the high frequency, low energy waves toward the low frequency, high energy waves as the coastal erosion continues (Fig. 10). Thus, Eq. 14 is solved discretely as:

$$E_m(j) = \sum_{i=1}^{n+1-j} \left[2M \int_{\alpha}^{\beta} \left\{ \left(\frac{u_{*m}}{u_{*c}} \right)^2 - 1 \right\} \left(1 - \frac{u_{*c}}{u_{*m}} \right) dt \right] P_{e,j}(i) \tag{15}$$

where j is the time step corresponding to the successive stages of $H_{e,min}$, and $P_{e,j}(i)$ is the distribution law of the Effective Scouring Wave at stage of j.

The variation of the Effective Scouring Wave is divided into eight stages ($n = 8$) in this study, which leads to an interval of 0.5 m for each $H_{e,min}$ (Fig. 10). $P_{e,j}(i)$ is obtained statistically from the wave height data of 1961-1973 in the Lianyungang Ocean Observation Station at the northern Huanghe Delta (Fig. 11). The erosion coefficient $M = 0.36\times10^{-4}$ kg/m^2.s (Yu et al., 1990) is used. The erosion rates with respect to different Effective Scouring Wave climates are calculated by Eq. 15. The results are shown in Fig. 12 and the relevant steady-state muddy profiles are illustrated in Fig. 13.

A steady-state muddy profile is related to a relevant Effective Scouring Wave climate. Fig. 13 demonstrates the evolution of the muddy profiles as a response to the variation of the Effective Scouring Wave climate. Several conspicuous features of the muddy profile evolution are seen in Fig. 13. Firstly, the profiles exhibit a concave upward profile pattern. As the coastal erosion proceeds, the profiles become more sharply concave upward. The maximum curvature always lies below the mean low tidal level. Obviously, the horizontal position of the maximum curvature is controlled by the maximum erosion rate caused by its relevant Effective Scouring Wave climate. Secondly, as the coastal erosion continues, the position of the maximum curvature moves down and shoreward, leading to a steeping of the sea floor on the shoreside of the maximum curvature and a flattening of the sea floor on the seaside of the maximum curvature. The width of intertidal zone decreases correspondingly. Thirdly, the rate of the profile evolution slows down as the Effective Scouring Wave becomes gradually restricted to higher energy, lower frequency waves. For instance, if the time spent on the evolution from the initial plane profile to profile 1, for which the Effective Scouring Wave consists of all waves in the local wave climate, is taken as a unit time, then the completion of the

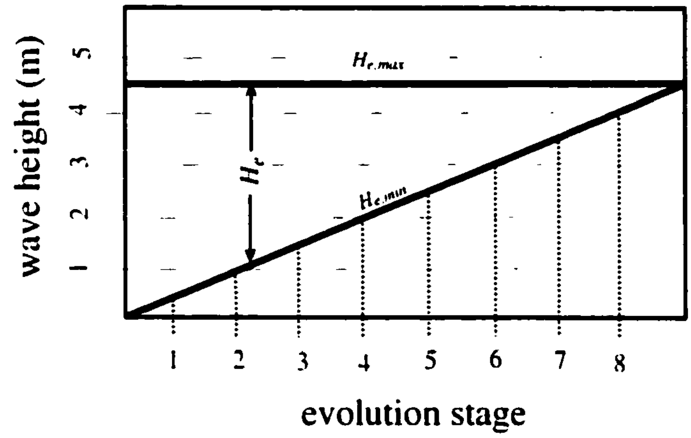

Fig. 10. Schematic drawing of the Effective Scouring Waves.

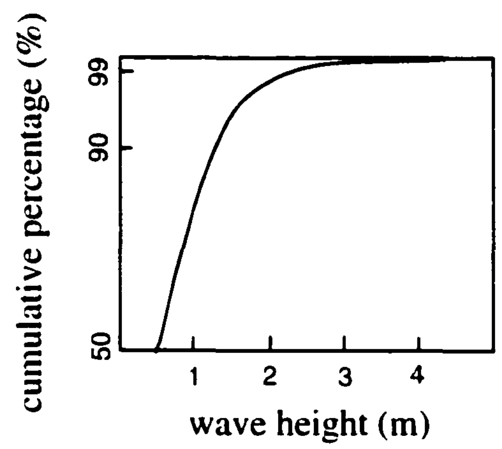

Fig. 11. Local wave climate (from the wave data at water depth of 8 m).

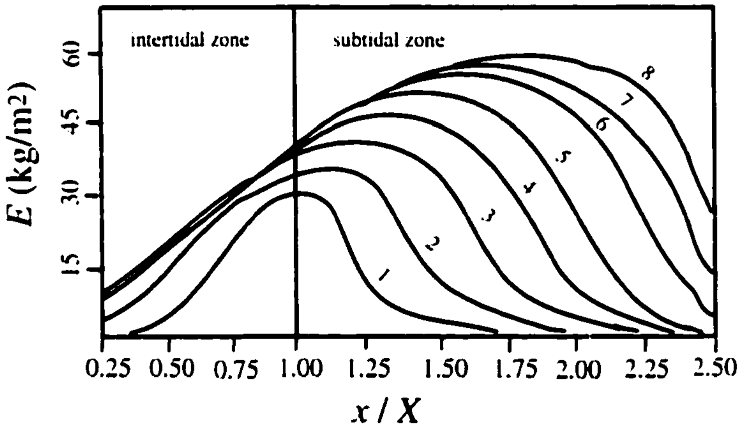

Fig. 12. Cross-shore distribution of erosion rates.

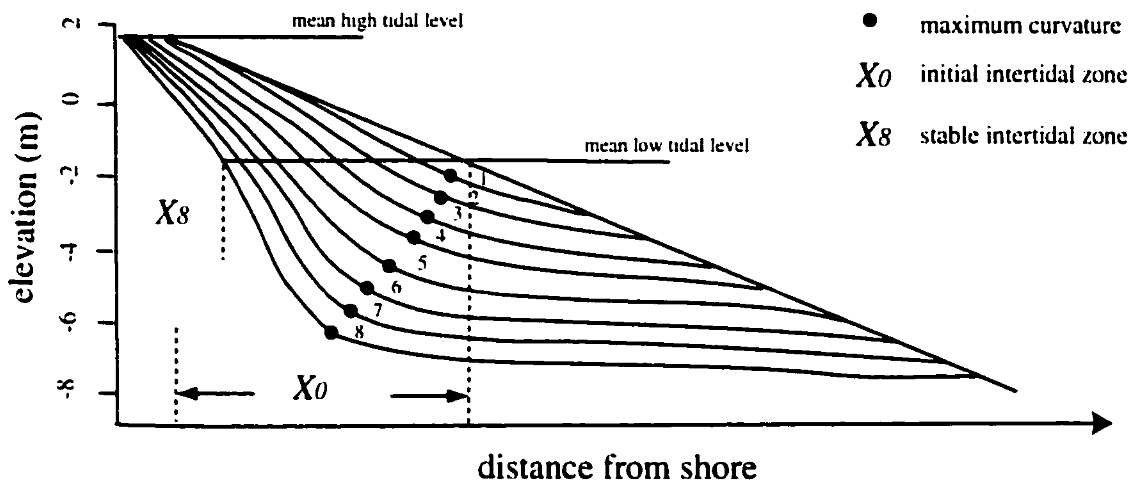
mean high tidal level
mean low tidal level
● maximum curvature
Xo initial intertidal zone
X8 stable intertidal zone
elevation (m)
2
0
-2
-4
-6
-8
X8
Xo
1
2
3
4
5
6
7
8
distance from shore

Fig. 13. Evolution of nearshore muddy profiles on the northern abandoned Huanghe Delta. The maximum curvatures of the muddy profiles are visually estimated.

evolution from profile 7 to 8 needs 3,140 units of time (Fig. 11). This is because the Effective Scouring Wave, at that evolutionary stage, is composed of those waves with a wave height of greater than 4.0 m and a frequency less than 0.03%. Finally, when the profile turns toward pattern 7 or 8, the position of the maximum curvature tends to be stable because of the much slower rate of the profile evolution at this stage. The profile thus approaches a final stable state.

DISCUSSION

This model simulates and predicts the muddy profile and its evolution in the northern abandoned Huanghe Delta, in which the coasts have been undergoing severe erosion since the shift of the Huanghe River in 1855. The model is constructed based on a theoretical framework in which the cohesive coast in the abandoned Huanghe Delta acts as a dynamical geomorphic system (Chorley et al., 1984). A nearshore muddy profile can be regarded as a steady-state profile that is mainly governed by a wave climate. However, for long-time scales, the nearshore muddy profile constitutes an irreversible evolutionary process. This is mainly a consequence of the time-variant nonlinearities of the system due to surface sand armoring and consolidating of mud substrate. The concept of the Effective Scouring Wave is proposed in order to quantitatively describe the effects of these geological nonlinearities in the system. By using the Effective Scouring Wave climate, the evolution of the nearshore muddy profile can be simulated and the ending equilibrium state can be predicted.

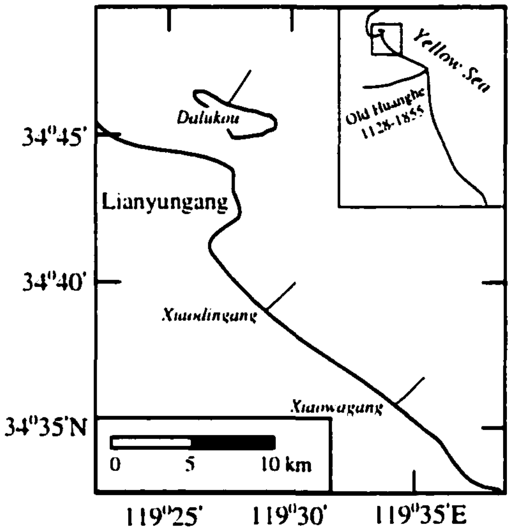
Dalukou
Lianyungang
Xiaoxlingang
Xiaowagang
Yellow Sea
Old Huanghe
1128-1855
34°45'
34°40'
34°35'N
0
5
10 km
119°25'
119°30'
119°35'E

Fig. 14. Location of field survey.

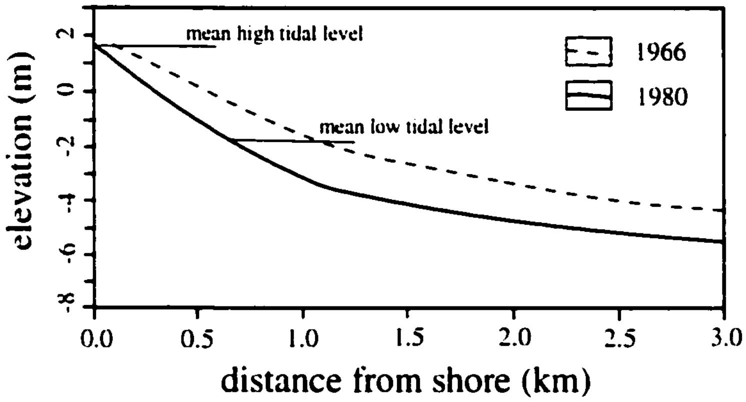

Fig. 15. Nearshore profile at Xiaodingang.

The data resulting from the field investigations of the study area are used to confirm the model. At Xiaodingang (Fig. 14), the muddy coast still undergoes severe erosion. For example, during the period of 14 years (1966-1980), the coastline at the mean high tidal level retreated 100 m, while the coastline at the mean low tidal level retreated more than 400 m, resulting in a reduction of the width of the intertidal zone from 900 m to 600 m, and the position of the maximum curvature moved down form 2.5 m to 3.5 m below the mean sea level (Fig. 15). The shape of the profile is equivalent to the theoretical profile 4 or 5 showed in the model (Fig. 13), which indicates that the evolution will continue, even though the erosion rate will be slower due to the thickening of the armoring sand layer on the top of the intertidal zone and the exposure of the older, well-consolidated cohesive sediments below it.

An even longer observation was taken at Xiaowagang (Fig. 14). The profile had almost the same pattern as that in Xiaodingang in the early of 1960's (Fig. 16). The most recent investigation shows that, after 28 years, the coastline at the mean high tidal level has retreated almost 200 m, and that in the mean low tidal level has retreated more than 700 m, leading to a reduction of the width of the intertidal zone from 900 m to 300 m, and a flattening of the profile in the subtidal zone. A downcutting of 1.5-2.0 m has occurred in the subtidal zone during 28 years (Fig. 16).

At Dalukou (Fig. 14), however, the situation is different. Because it is located in the far end of the northern abandoned Huanghe Delta, and because a considerable amount of sand has been provided by the erosion of nearby rocky bluff, the intertidal zone has almost been covered by sands. The sand layer extends down more than 1 m below the surface at the upper part of the intertidal zone. The field survey illustrates that the maximum curvature of the profile was located in about 4.0 m depth in 1936, and moved down to 4.8 m depth below mean sea level after 26 years of erosion (Fig. 17). The erosion rate slowed significantly during two decades with the maximum curvature moving further down to 5.2 m depth. The shape of the profile almost matches the profile pattern 7 in Fig. 13, implying that a stable, or equilibrium state has almost been approached in this area.

The behavior of modeled coastal profiles on the abandoned Huanghe Delta is compatible with observations made on other delta coasts (Curray, 1969). Repeated river avulsion, leading to a cycle of growth and abandonment of successive deltas (usually referred to as subdeltas) is a characteristic of most delta systems. On the Mississippi Delta (Coleman, 1988), delta building occurs over several space and time scales. Large subdeltas (2,000 km^3) form and are abandoned within 2,000 years, whereas the small subdeltas (200 km^3) exhibit life cycles of 200 years or less. The muddy western Louisiana coast, downstream from the Mississippi Delta has a history of intermittent progradation, that is at least partly controlled by the growth cycles of the delta to the west. Similar cycles of progradation and erosion characterize the muddy coasts west of the Amazon Delta (Wells and Coleman, 1981) and west of the Ord Delta of Australia (Rhodes, 1982), and patterns of coastal profile re-establishment, similar to those observed and modeled in the abandoned Huanghe Delta region, may be expected in these areas also.

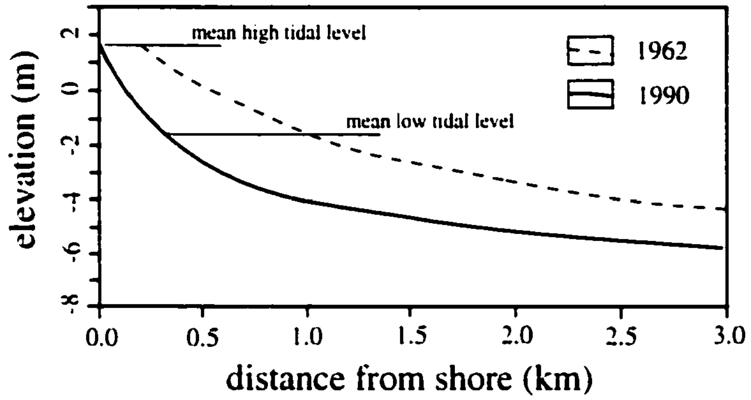

Fig. 16. Nearshore profile at Xiaowagang

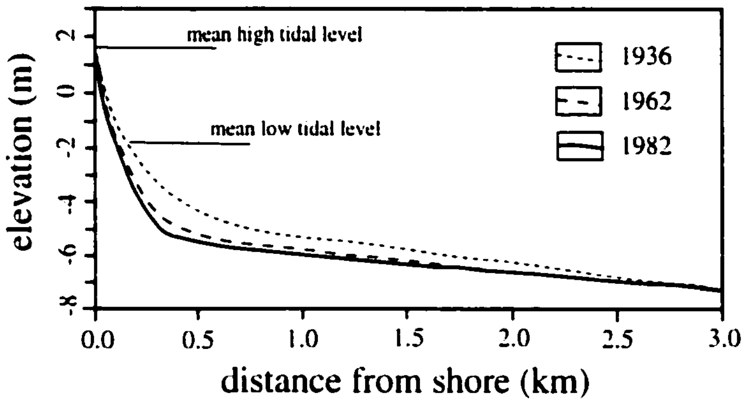

Fig. 17. Nearshore profile at Dalukou

CONCLUSIONS

This chapter presents a dynamical model designed to simulate and predict the evolution of the nearshore muddy profiles in the abandoned Huanghe Delta. The mechanism of tidal sea level fluctuation in re-distribution of the wave-induced bed shear stress has been accounted for in the model. The cohesive coast in the study area behaves as a dynamical geomorphic system. A steady-state muddy profile is determined by the average erosion rate of the local wave climate. However, at long-time scales, the wave-induced erosion rate is significantly influenced by surface sand armoring and the vertical increase with depth of consolidating of the muddy substrata. The concept of the *Effective Scouring Wave* is proposed to quantify these time-variant geological influences. Using this concept, this model simulates the evolution of the nearshore muddy profile and predicts the ultimate steady-state configuration of the muddy profile in the northern abandoned Huanghe Delta.

Profiles on eroding muddy coasts are exponentially curved and concave upward. The degree of curvature increases as the coastal erosion continues. The maximum curvature of the profile lies below the water depth of mean low tidal level. As erosion proceeds, the position of the maximum curvature of profile moves down and shoreward, resulting in a steeping of the sea floor shoreward of the position of the maximum curvature, and a flattening of the sea floor seaward of the position of the maximum curvature. As the coastal erosion continues, the erosion rate decreases due to the increasing influence of surface sand armoring and the vertical increase with depth of mud consolidation, and so does the downward movement of the point of maximum curvature. In the northern abandoned Huanghe Delta, the muddy profile approaches an equilibrium state when the maximum curvature reaches down to a water depth of about 6-7 m below the mean sea level. The profile evolution simulated and predicted by the model in the abandoned Huanghe Delta may suggest the similar profile pattern and the evolution process observed in other abandoned delta coasts with dominantly fine-grained sediments.

CHAPTER III

TWO-DIMENSIONAL NUMERICAL MODELING OF STORM DEPOSITION ON THE NORTHERN CALIFORNIA SHELF

INTRODUCTION

Rare but energetic events such as ocean storms and river floods dominate sedimentation on most continental margins. During storms, sediments on the sea floor are resuspended, transported and redeposited as a response to the bottom oscillatory flow induced by surface waves and the mean current over a few hours or days duration. In recent years, many models have been developed for shelf sediment transport (Lyne et al., 1990; Wiberg et al., 1994; Green et al., 1995). However, these one-dimensional models focused only on the sediment resuspension and the maximum erosion depth at a single location. This chapter describes a two-dimensional, across-shelf sediment transport model that has been developed to simulate storm deposition on the Eel shelf, Northern California (Fig. 18). In the model, time-dependent sediment resuspension, transportation, deposition, and their across-shelf variations with respect to storm waves, are simulated. Thus, storm-bed generation is quantitatively modeled, and different mechanisms driving across-shelf sediment transport are investigated, providing dynamical insights into shelf

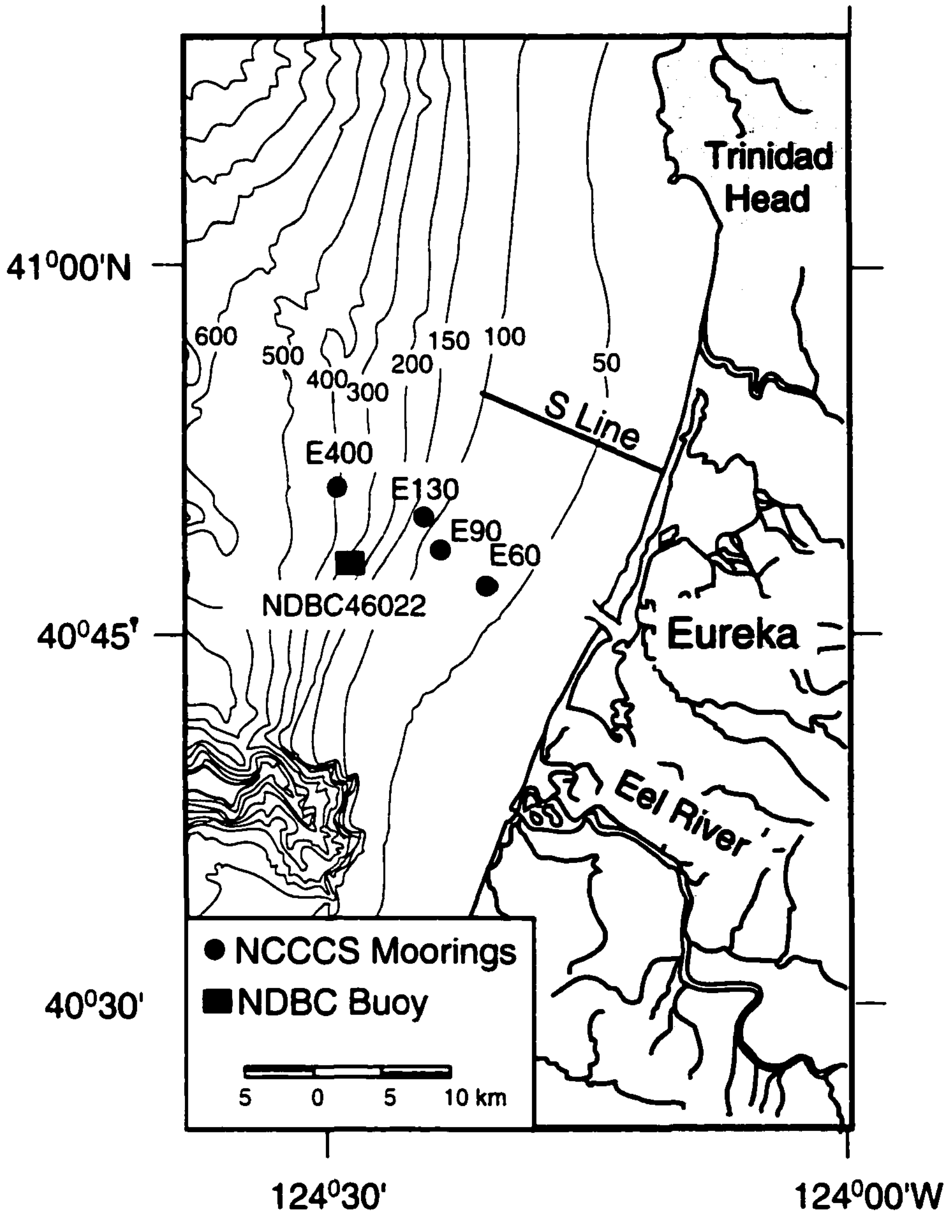
Trinidad Head
41°00'N
600
500
400
300
200
150
100
50
S Line
E400
E130
E90
E60
NDBC46022
40°45'
Eureka
Eel River
40°30'
● NCCCS Moorings
■ NDBC Buoy
5 0 5 10 km
124°30'
124°00'W

Fig. 18. Location of study area. The S Line is the transect on which the model simulation is conducted.

sedimentation. Furthermore, this model, combined with the flood-bed simulation, can be extended to the simulation of bed successions or lithofacies with respect to storm climate and flood climate (Carey et al., 1999). Dynamical linkage between two scales of numerical simulation, from a deterministic scale (individual bed or event scale) to a stochastic scale (bed-succession or facies scale), can be approached through computation of the event bed preservation potentials (Zhang et al., 1997).

STORM-DEPOSITION MODEL

Conceptual Model

Fig. 19 presents a conceptual model of storm-bed generation on continental shelves. The conceptual model serves as a framework to which the physics of sediment transport is attached for the purpose of modeling. Sediments on the sea floor are resuspended by wave-current combined flow in the benthic boundary layer, and are transported as a graded suspension by a net across-shelf current during storms. These suspended sediments are then progressively redeposited on the sea floor as the storm wanes, and hence form a size-graded storm bed resting on a basal diastem.

Governing Equations

The suspended-sediment concentrations are calculated from a mass-balance equation in an across-shelf section (*x*-*z* plane):

$$\frac{\partial C}{\partial t}+\frac{\partial U_x C}{\partial x}-\frac{\partial}{\partial x}\left(\varepsilon_x\frac{\partial C}{\partial x}\right)-W_s\frac{\partial C}{\partial z}-\frac{\partial}{\partial z}\left(\varepsilon_z\frac{\partial C}{\partial z}\right)=0 \tag{16}$$

where x is the across-shelf distance positive towards the sea with its origin at the coastline, z is the vertical distance positive upward with its origin at the pre-storm water-sediment interface, C is the mass sediment concentration, U_x is the across-shelf component of subtidal current velocity, W_s is the settling velocity of suspended sediment, ε_x and ε_z are the sediment eddy diffusivities in x and z directions respectively. Suspended-sediment concentrations can be calculated by numerically solving Eq. 16 when the across-shelf current U_x, sediment eddy diffusivities ε_x and ε_z, sediment settling velocity W_s, and relevant boundary conditions are given or appropriately specified.

Once the time- and space-variant sediment concentration field is known, across-shelf sediment flux can be computed. Thus the change of sea-floor height can be calculated by the mass continuity equation:

$$\frac{\partial z_b}{\partial t}=\frac{1}{c_b\rho_s}\left(\frac{\partial C_T}{\partial t}+\frac{\partial U_x C_T}{\partial x}\right) \tag{17}$$

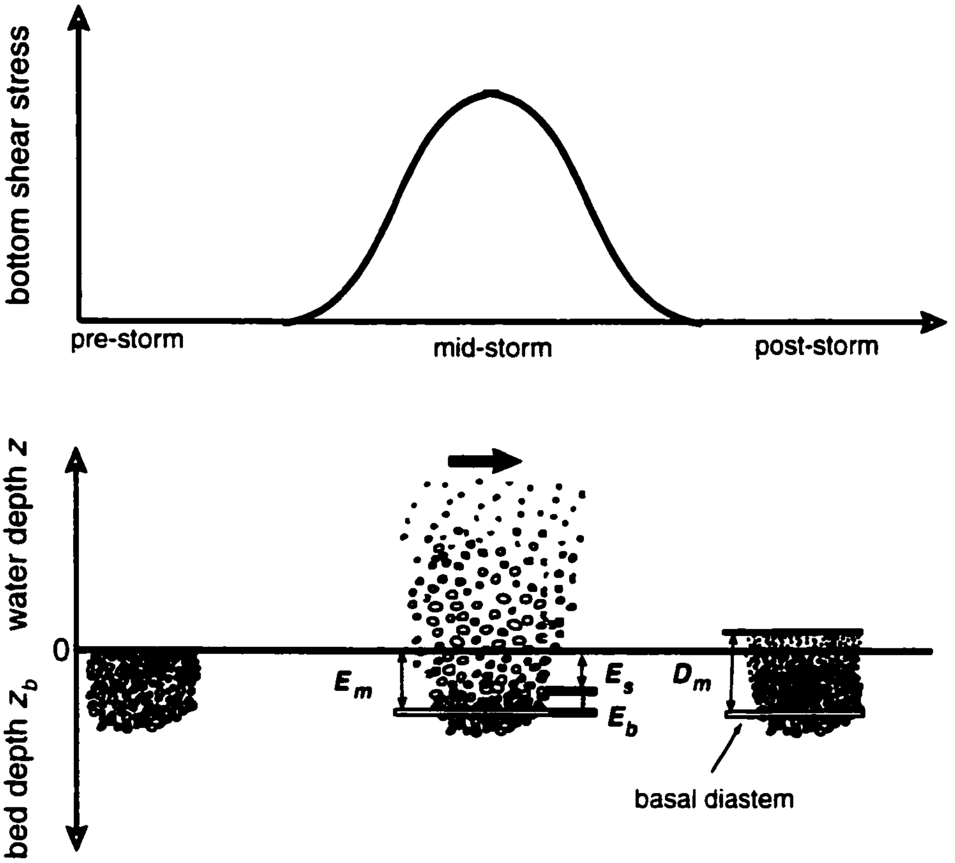
bottom shear stress
pre-storm
mid-storm
post-storm
bed depth z_b
water depth z
0
E_m
E_s
E_b
D_m
basal diastem

Fig. 19. A conceptual model of storm deposition on continental shelf. E_b is the erosion depth for bedload transport, and E_s is the erosion depth for suspension transport, and E_m is the maximum erosion depth. D_m is thickness of storm bed.

where z_b is the sea floor elevation (positive downward), c_b is the volume sediment concentration of seabed, ρ_s is the sediment density, and C_T is the depth-integrated mass sediment concentration.

The Eel shelf is covered by mud deposits on the middle and the outer shelf (Borgeld et al., 1999). Consequently, bedload transport is a possible mode only on the inner shelf, where the seabed is composed mainly of the noncohesive sediments. Field investigations on continental shelves show that suspended sediments often dominate sediment transport (Dyer and Soulsby, 1988). A simple equation, proposed by Nielsen (1992), is used to calculate the thickness of the bedload layer at rest:

$$L_b = 2.5(\theta - \theta_c)d \tag{18}$$

where L_b is the thickness of bedload layer, θ and θ_c are the effective Shields parameter and the critical Shields parameter respectively, and d is the sediment grain diameter.

A storm bed is created after a storm. The bottom boundary of a storm bed corresponds to the maximum erosion depth on a mixed bed, E_m, that is:

$$E_m = E_b + E_s \tag{19}$$

where E_b is the maximum erosion depth caused by bedload movement and E_s is the maximum erosion depth caused by resuspension of bottom sediments. E_b is determined by Eq. 18 and E_s is determined by Eqs. 16 and 17 with respect to the maximum bottom shear stress during a storm. The upper boundary of a storm bed is determined by:

$$D_m = D_s + D_b \tag{20}$$

where D_m is the maximum thickness of the bed deposited after a storm, D_s is the maximum deposited thickness of suspended sediment determined by Eqs. 16 and 17, and D_b is the maximum deposited thickness of bedload sediment. Considering that the bedload movement is mainly dominated by the oscillatory flows caused by surface waves during strong storm events, the spatial gradient of bedload flux can be reasonably neglected (Niedoroda et al., 1989). Thus, D_b is equal to E_b. Eqs. 19 and 20 describe the across-shelf geometry of a storm bed.

Algorithms for Important Processes on Storm-bed Formation

In order to solve Eqs. 16 and 17 for the cross-shelf sediment transport and bed evolution, the values of the advection and diffusion terms need to be specified. The basic numerical solution algorithm consists of specifying the currents, diffusion and suspended sediment concentration profiles at each instant (time step) based on time-series of measured values of the current and wave parameters at a few points.

Wave-current boundary layer

The simultaneous existence of surface waves and currents during storm results in a small-scale wave boundary layer embedded in a large-scale current boundary layer.

Information concerning the combined storm and current boundary layer is essential for the analysis of near-bottom current flow and sediment suspension. Models for flow structures inside and outside the wave-current boundary layer have been developed during the last two decades (Grant and Madsen, 1979; 1986; Sleath, 1991; Eidsvik, 1993; You, 1994). However, differences in time and space scales make it difficult to directly couple these boundary models into our larger-scale numerical sediment-transport model. For example, the vertical grid in the numerical solution of the larger-scale sediment-transport model is usually much larger than the thickness of the wave boundary layer. The high-resolution current structure within the wave boundary layer of a two-layer model as described for instance by Grant and Madsen (1979), cannot be easily and explicitly represented in a larger-scale sediment-transport model.

The current profile above the wave-current boundary layer is determined using a log-layer profile and apparent roughness due to the presence of the waves. The equation for apparent roughness proposed by Sleath (1991) is used:

$$z_a = z_0\left(1 + 0.19\frac{u_b}{u_{*c}}\sqrt{\frac{u_b}{30 z_0 \omega}}\right) \tag{21}$$

where z_a is the apparent roughness, z_0 is the hydraulic roughness, u_b is the maximum wave orbital velocity near the bottom and u_{*c} is the shear velocity of the current. Thus, the current profile U_z above wave-current boundary layer is:

$$U_z = \frac{u_{*c}}{\kappa} \ln \frac{z}{z_a} \tag{22}$$

where κ is von Karman's constant. For a given mean current velocity U_{ref} at $z = z_{ref}$ (where z_{ref}> wave-current boundary layer δ) within the near-bottom logarithmic part of the current profile, the values of u_{*c} and z_a can be calculated by solving Eqs. 21 and 22 using an iterative procedure. Therefore, the current profile above the wave-current boundary layer is determined. The bottom hydraulic roughness z_0 is $k_b/30$, in which k_b is estimated through the equation suggested by Xu and Wright (1995):

$$k_b = d + 8\eta\left(\frac{\eta}{\lambda}\right) + \Omega d(\theta - \theta_c) \tag{23}$$

where η and λ are the sand ripple height and length, respectively, and Ω is the scaling constant. The sand ripple height and length are determined by the procedure proposed by Nielsen (1981).

In the model, the wave-current boundary layer is treated as a bottom grid layer. Its thickness is a time-varying value defined as $\delta = 2u_{*w}/\omega$, as suggested by Grant and Madsen (1986). Here, δ is the thickness of wave-current boundary, u_{*w} is the shear velocity caused by the waves and ω is the wave radian frequency. The value of u_{*w} is determined using a friction factor formulation suggested by Swart (1974). The current velocity (U_δ) and the suspended-sediment concentration (c_δ) at the top of wave boundary layer are calculated, based on an equilibrium assumption concerning the wave boundary layer such that:

$$U_\delta = \frac{u_{*c}^2}{u_{*wc}\kappa} \ln\left(\frac{\delta}{z_0}\right) \tag{24}$$

and:

$$c_\delta = C_a\left(\frac{\delta}{z_0}\right)^{-(\omega / \kappa u_{*wc})} \tag{25}$$

where C_a is the reference sediment concentration at z_0, u_{*wc} is the combined shear velocity in the wave-current boundary layer that is assumed to be equivalent to u_{*w} (as suggested by You, 1994). The error caused by this approximation is within the same order of magnitude as other errors induced by the assumption of equilibrium (Bedford and Lee, 1994) and by the numerical solution method.

Multi-grain-size bed

The natural sea floor is characterized by a mixed bed, which consists of a range of sediment grain sizes. For a given flow condition, selective entrainment, commonly referred to as bed armoring, may take place on a mixed bed due to the different resistance of sediment grain sizes to erosion (Reed et al., 1999). How to relate the simulations of sediment transport to a mixed bed is a matter of considerable importance in modeling storm deposition on continental shelves. This is particularly true for the Eel shelf where the sea floor is covered by sediments ranging in grain size from sand to clay.

If all sizes of sediments are removable, the relationship between erosion depths in a mixed bed and that in a single-size bed, in accordance with the mass continuity, is:

$$A_i E_m = B_i E_i \tag{26}$$

where, A_i is the fractional percentage of ith-class sediment in a mixed bed, E_i is the erosion depth of single-size bed consisting only of ith-size class sediment under the same flow condition. Rewriting Eq. 26 yields:

$$B_i = \frac{A_i E_m}{E_i} \tag{27}$$

Obviously, B_i is not equal to A_i unless $E_m = E_i$, which is only possible when the mixed bed has become a single-size bed, consisting only of ith-size class sediment. B_i presents the percentage of eroded sediments in a single-size bed. This amount of sediments should be identical to the amount of ith-size sediments that are really moved in E_m, if the single-size bed and the mixed bed are subjected to the same flow conditions. Summing of both sides of Eq. 27 yields:

$$\sum_{i=1}^{N} B_i = E_m \sum_{i=1}^{N} \frac{A_i}{E_i} \tag{28}$$

where, N is the number of sediment size classes. Shi et al. (1985) first proposed Eq. 28, but identified B_i as the fraction of ith-size component in a poorly defined "near-bed" region. The total energy that acts on a mixed bed as presented by the sum of various energy ratios, B_i, should be equal to one. This yields the following equation for the erosion depth of a mixed bed:

$$E_m = \left(\sum_{i=1}^{N} \frac{A_i}{E_i} \right)^{-1} \tag{29}$$

If all sizes of sediments are not removed during storms, an armored layer will develop, resulting in stopping of further erosion. Under such an armoring condition, sediments and flow dynamics cannot reach equilibrium, so Eq. 29 is not applicable. The erosion depth for such a situation can be calculated in terms of an upper-bed layer known as the active layer (Thomas and Prasuhn, 1977), in which unmovable particles remain to cover the entire bed surface. The equation of the active layer thickness (Borah et al., 1982), is used here to determine the erosion depth:

$$E_m = \frac{D_a}{c_b A_a} \tag{30}$$

where D_a is the smallest unmovable size in an armor layer, and A_a is the fraction of all unmovable sediments in a mixed bed.

Boundary Conditions

Initial conditions

The initial sea-floor profile is located along the S transect (see Fig. 18). The initial sea bed is assumed to be well-mixed. The bottom sediments on the middle and the outer shelf are specified by interpolating the STRATAFORM data collected during November of 1995 (J.C. Borgeld, personal communication). The sand compositions on the inner shelf are derived from the field survey data represented by Borgeld (1985). The initial (pre-storm) suspended-sediment concentrations are specified as zero over the simulated transect.

Coastal boundary and shelf-break boundary

The coastal boundary provides a seaward sediment flux from the nearshore zone during storms. A realistic sediment flux is difficult to specify without knowledge of the nearshore sediment transport and therefore a zero-flux profile is selected. The shelf-break boundary is set at a depth of 100 m, about 15 km from shore. At this open boundary, the Sommerfeld radiation condition is selected (Camerlengo and O'Brien, 1980; Roed and Smedstad, 1984) based on the assumption that sediment transport on the continental slope and beyond has little influence on the shelf storm deposition.

Upper boundary

Many field measurements have indicated that suspended-sediment transport mainly occurs within a few meters above the sea floor on continental shelves (Bedford and Lee, 1994; Wright et al., 1994, Green et al., 1995; Cacchione et al., 1999). An upper limit of 20 m from bottom has been selected in our model as a thickness of the sediment-transport layer. The vertical sediment flux at the upper boundary of the transport layer is assumed to be zero, which leads to:

$$-W_s C + \varepsilon_z \frac{\partial C}{\partial z} = 0 \tag{31}$$

Bottom boundary: noncohesive sediments

Two options for sediment input at the bottom boundary are available in the model. For a sand bed, a reference sediment concentration C_a at z_0 is generally formulated as (Smith and McLean, 1977):

$$C_a = c_b \frac{\gamma_0 \theta'}{1 + \gamma_0 \theta'} \tag{32}$$

where c_b is the bed sediment concentration, γ_0 is the resuspension coefficient, and θ' is the wave-period-averaged excess skin friction $\theta' = (\theta - \theta_c)/\theta_c$. Reported values of the resuspension coefficient γ_0 vary over two orders of the magnitude (Nittrouer and Wright, 1994). Here, a constant value of 2.4 x 10^{-3}, suggested by Smith and McLean (1977), has been used in our model. When waves are present, the bottom grid point in the water column in the numerical solution is set at the top of the wave-current boundary layer at height δ off the bottom, and the concentration is specified by Eq. 25.

Bottom boundary: cohesive sediments

Most of our study area, from the middle to the outer shelf, consists of mud deposits (Borgeld et al., 1999). The primary source of these cohesive sediments is the

Eel River (Wheatcroft et al., 1997). Computations of cohesive sediment transport are undertaken in a manner that differs from computations of sand transport (Mehta et al., 1989; Teisson et al., 1993; Partheniades, 1993). Empirical formulations are still widely used in simulation of cohesive sediment transport. Parameters related to sediment properties are generally based on site-specific field measurements or laboratory experiments. The deposition rate of mud is given by Krone (1962) and Odd and Owen (1972) as:

$$\frac{dM_d}{dt} = pW_dC_b \tag{33}$$

where dM_d/dt is the sediment mass deposited per unit area per unit time, W_d is the settling velocity of the flocs, C_b is the suspended sediment concentration just above the water-sediment interface, and p is the probability that cohesive particles will stick to the bed. Krone (1962) found that p can be expressed as:

$$\begin{array}{ll} p = 1 - \dfrac{\tau_b}{\tau_d} & \tau_b \le \tau_d \\ p = 0 & \tau_b > \tau_d \end{array} \tag{34}$$

where τ_b is the bottom shear stress and τ_d is the critical bottom shear stress for deposition. For San Francisco Bay mud, Krone (1962) found that τ_d is 0.06 N/m^2, when the initial suspended- sediment concentration is less than 0.3 kg/m^3. This value is used in the model due to the lack of equivalent measurements for the Eel shelf mud. The relationship between the erosion rate and the bottom shear stress is described by Partheniades (1965) as:

$$\frac{dM_e}{dt} = E\left(\frac{\tau_b}{\tau_e} - 1\right) \qquad \tau_b \geq \tau_e$$
$$\frac{dM_e}{dt} = 0 \qquad \tau_b < \tau_e \tag{35}$$

where dM_e/dt is the mass eroded per unit area per unit time, E is the erosion constant, and τ_e is the critical bottom shear stress for erosion. Reported values of E and τ_e vary over a significantly wide range due to the site-specific character of cohesive sediments. In the absence of both field and laboratory experiments on the erosion parameters of the Eel shelf mud, a value of $\tau_e = 0.2$ N/m^2, the lowest value of the critical shear stress with least biological influence measured by Schunemann and Kuhl (1993), is used for our simulations. The erosion constant $E = 6.25 \times 10^{-7}$ g/cm^{2}s, measured by DeVries (1992) for the mud from Mare Island Strait, California, is used in the simulations.

The upward sediment flux is used to specify the bottom-boundary condition on mud beds. Net erosion and deposition are mutually exclusive in cohesive sediment transport (Ariathurai and Krone, 1976; Partheniades, 1986, 1993; Mehta et al, 1989). The critical shear stress for erosion τ_e is greater than the critical shear stress for deposition τ_d. Unlike sand, for which deposition immediately occurs when bottom shear stress decreases, an intermediate range of bottom shear stress for mud can exist for which neither erosion nor deposition occurs. This deposition-nondeposition-erosion paradigm is adopted in the model for mud transport:

$$-W_sC+\varepsilon_z\frac{\partial C}{\partial z}=-\frac{dM_d}{dt} \qquad \tau<\tau_d$$

$$-W_sC+\varepsilon_z\frac{\partial C}{\partial z}=0 \qquad \tau_d<\tau<\tau_e \qquad (36)$$

$$-W_sC+\varepsilon_z\frac{\partial C}{\partial z}=-\frac{dM_e}{dt} \qquad \tau>\tau_e$$

where dM_d/dt and dM_e/dt are derived from Eqs. 33 and 35 respectively.

Current Field

During STRATAFORM Project, two tripods from VIMS were deployed at depths of 60 m and 70 m along the S transect (Wright et al., 1999). Comparison of the measured current speed during winter season with the significant wave height from the nearby buoy NDBC46022 (see Fig. 18) clearly shows that there is little correlation between them (Fig. 20). The low-frequency subtidal current near the bottom is offshore-dominant.

Systemic observations of wind forced currents were conducted by the Northern California Coastal Circulation Study (NCCCS) during 1988 to 1989 along the northern California Shelf. A mooring transect, consisting of four moorings (at water depths of 60 m, 90 m, 130 m, and 400 m, see Fig. 18), was deployed on the Eel shelf during the experiment, from which the independence of waves and currents on the Eel shelf was observed by Largier et al. (1993). The same situation was found during the Sediment Transport Events on Shelves and Slopes (STRESS) project on the shelf 150 km south of the Eel shelf (Sherwood et al., 1994). The waves that cause sediment resuspension and currents that determine sediment transport are independent phenomena. The across-shelf component of the low-frequency subtidal current, which is responsible for the across-shelf sediment flux, is poorly related to the wave height on the Eel shelf.

In order to model storm deposition in a setting where the wave height and the mean current velocity are poorly correlated, it is necessary to provide an independent current field within the bottom friction layer. The STRESS measurements showed that the mean current velocities at 1 m above bottom had an average value of less than 10 cm/s across the shelf from water depths of 50 m to 130 m (Sherwood et al., 1994). The across-shelf variation of the mean current velocities is also showed to be small, particularly at the water depths shallower than 100 m. In this case, the mean current velocity at 1 m above bottom is specified from the field data as a background value during storms. A value of 20 cm/s at 1 m above bottom, which approximately represents the average peak value for the mean current velocities in the VIMS tripod measurements (see Fig. 20) is selected for the calculation of the shear stress in our model. A time-invariant, offshore subtidal velocity of 2 cm/s is selected for the calculation of the sediment flux in our model (Fredericks et al., 1993).

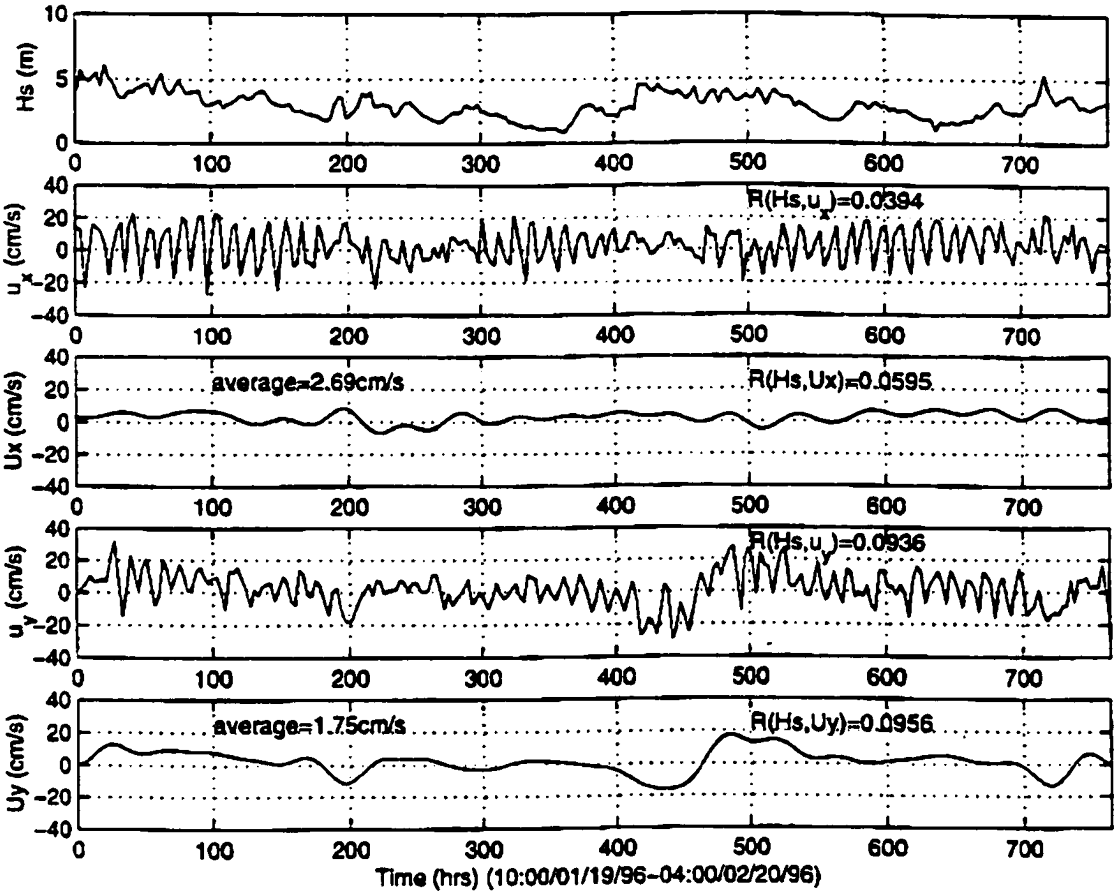

Fig. 20. Measurements at 101 cm above the sea floor in 60 m water depth (VIMS S60). H_s is the significant wave height at NEBC46022. The parameter u_x is the across-shelf component of mean current velocity, u_y is the along-shelf component of mean current velocity. U_x is the across-shelf component of subtidal current velocity, and U_y is the along-shelf component of subtidal current velocity.

Other Parameters

Sediment eddy diffusivities

The vertical and horizontal sediment eddy diffusivities are $\varepsilon_z = \varepsilon_x = \beta\varepsilon_m$. Here, ε_m is the water eddy viscosity:

$$\begin{aligned} \varepsilon_m &= \kappa u_{*c} z & z &< \delta_e / 10 \\ \varepsilon_m &= \kappa u_{*c} z_\delta & z &\geq \delta_e / 10 \end{aligned} \tag{37}$$

where δ_e is the thickness of the bottom Ekman layer, z_δ is the elevation at $\delta_e/10$. The value of β is suggested by Dyer and Soulsby (1988) to be equal to 1 on continental shelves.

Wave parameters

An empirical equation (Tucker, 1991) for the mean zero-crossing period of waves during storms, $T = 3.4\ H_{s,d}^{1/2}$, is used in our model. Here, $H_{s,d}$ is the significant wave height in deep water. The transformation of the wind wave, owing to the bottom friction when it travels into the shallow water, is estimated by the wave transformation equation proposed by Hughes and Miller (1987):

$$H_s = H_{s.d}\left(\frac{L_s}{L_{s.d}}\right)^{\frac{3}{4}} \tag{38}$$

where $H_{s,d}$ and $L_{s,d}$ are the significant wave height and length in deep water, respectively.

Settling velocities for muds

The transport behavior of cohesive sediments is significantly affected by the processes of physico-chemical flocculation and biological agglomeration (Mehta et al., 1989; Teisson et al., 1993; Berlamont et al., 1993). The size and settling velocity of the aggregates, which are the most common forms for cohesive sediments in the marine environment, depend largely on the flow shear stress and sediment concentration (Burban et al., 1990; Van Leussen, 1988). As part of the STRATAFORM Program, an *in situ* measurement of particle size and settling velocity has been conducted by Sternberg et al. (1996), from which an average settling velocity of 0.06 cm/s for various aggregates is adopted in the model.

Numerical Solution

The sediments are divided into 5 categories of grain size, which are coarse sand (0-2 ϕ), fine sand (2-4 ϕ), coarse silt (4-6 ϕ), fine silt (6-8 ϕ) and clay (>8 ϕ). The boundary between sand and mud is set at 4 ϕ in the model. For each grain size, the time-varying suspended-sediment concentration, and hence the sea-floor elevation are calculated by using the finite difference method to solve Eqs. 16 and 17. The algorithm for mixed bed is then applied in the simulations. A grid of 100 nodes in vertical direction with a space step of 0.2 m and 300 nodes in horizontal direction with a space step of 50 m is designated. The change of the sea-floor elevation is reduced to 1% when the time step is 15 minutes. A storm event of 20-year return period, with a maximum significant wave height of 10.1 m and a storm duration of 2.3 days (from NDBC46022 buoy data), is used in our simulation. The wave height is assumed to increase linearly as the storm waxes and decrease linearly as the storm wanes. A wave height of 2.0 m is selected as the background wave (non-storm wave), with which the storm starts and ends. The computation time has been extended to one day after the storm, in order to account for the possible deposition caused by flow-sediment hysteresis effect for mud.

COMPUTATIONAL RESULTS

Several experiments have been undertaken with different values of the hydraulic and sediment parameters that are usually considered to be responsible for across-shelf sediment transport. Across-shelf variations of the thickness of storm beds reveal a general pattern of storm deposition on the Eel shelf (Figs. 21 and 22). Storm-bed character is dependent on pre-storm bottom sediment composition. On the inner shelf where sand deposits dominate (>90%), storm-bed thickness attains a peak value at the coastal boundary and progressively decreases seaward to the 50-m isobath, 6 km offshore. Farther seaward, the bottom becomes muddy, and the thickness of storm beds begin to increase owing to the reduced erosion resistance of the mud, despite the progressive weakening of bottom wave power as water depth increases. The maximum bed thickness is located at about 10 km from shore, in the water depth of 70 m. Beyond this depth, bed thickness decreases again, as the decreasing wave orbital velocity becomes the dominant control.

It is noteworthy that the locus of maximum storm bed thickness predicted by the model was the site of new beds found three weeks after the Eel River flood in January of 1995 (Wheatcroft et al., 1997). There is clear evidence that the muddy sediments of this lenticular deposit, centered on the 70 m isobath, came from the Eel River (Wheatcroft et al., 1996, 1997). However, little dynamical evidence has been found to interpret the shelf dispersal system that formed the deposition. The NDBC46022 buoy data indicates that there were several big storms in January of 1995 with a maximum wave height of 8.2 m in the Eel shelf. In addition, the dispersal of the mud-rich and cohesive Eel River flood sediments is also controlled by the consolidation process. Newly deposited cohesive sediments usually form a fluid-mud layer that is easily reworked and transported even by high-frequency tidal currents. The deposition of the flood sediments must thus be a time-varying process, significantly affected by oceanic forces. There is a strong coherence between floods and winter storms in the Eel shelf (Wheatcroft et al., 1997). The model here suggests that the across-shelf variability of the deposition and the structure of the deposited beds be most likely controlled by the storm waves during the storm-flood event. While the source of its material was a inshore flood plume (Wheatcroft et al., 1997), the beds of January of 1995 appear to have been storm-transported to the site of deposition. The geometry and thickness presumably reflects such storm parameters as maximum wave height and suspended sediment concentration in the benthic boundary layer, rather than the sediment concentration and duration of the plume. Since the 1995 flood deposit consists of several discreet beds, inshore flood deposits appear to have reworked, transported and redeposited several times by storm waves and other oceanic forces after being discharged from the Eel River.

The numerical experiments of the model show that the position of maximum thickness of storm beds in the mud zone is mainly determined by the pre-storm sediment composition of the sea floor (Fig. 23). Its value, however, varies with the bottom oscillatory flow of storm waves that increases toward the shore. The simulations indicate that as the mean current velocity and the net seaward subtidal current increase, the storm-bed thickness will increase accordingly, particularly in the middle and the outer shelf mud zone (Fig. 21). Under conditions of unidirectional seaward flow, sand is eroded on the inner shelf, and deposited on the middle shelf in the water depths of 45-55 m (Figs. 21 and 22), where an interstratified sand and mud facies is found. However, the advected quantities are small in comparison with the amount produced by *in situ* winnowing. The advected quantities of sand may be underestimated because the littoral sediment input is not included in the computation. An increase in the mean current velocity and the net seaward subtidal current leads to net erosion occurring at a depth of 60-75 m and net deposition deposition at a depth of 75-84 m (Fig. 21) during the storm event.

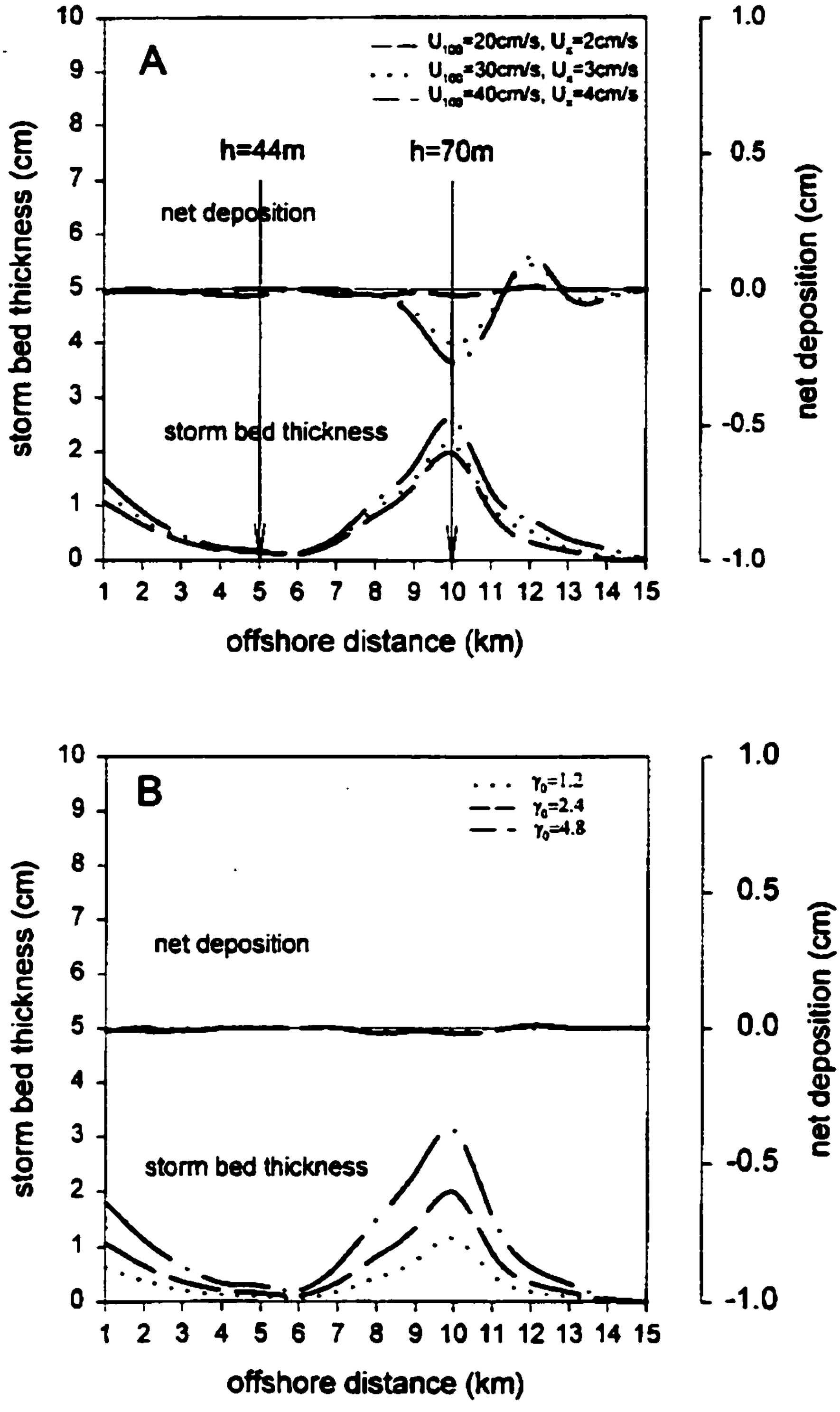

Fig. 21. (A) Storm-bed thickness as a function of current velocity, and (B) storm-bed thickness as a function of γ_0.

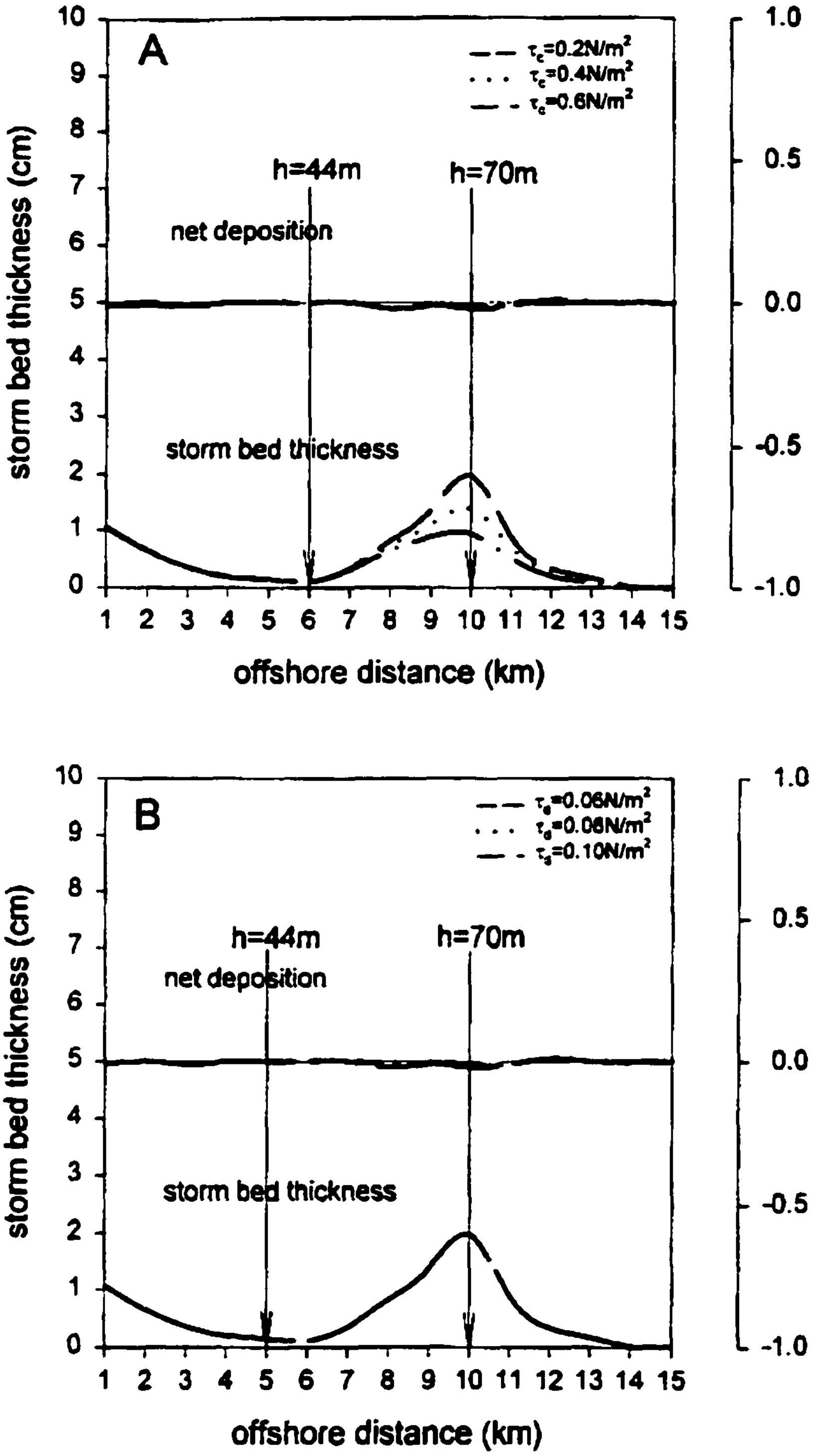

Fig. 22. (A) Storm-bed thickness vs. critical shear stress for mud erosion, and (B) critical stress for mud deposition.

Sensitivity experiments demonstrate that the critical bottom shear stress for mud erosion, τ_e, is more important than the critical bottom shear stress for mud deposition, τ_d, in determining the thickness of muddy storm beds (Fig. 22). For sand deposits, the resuspension coefficient, γ_0, is more important than the bottom roughness scaling constant, Ω, in determining the thickness of sandy storm bed. A decrease in γ_0 leads to a decrease in sand resuspension and deposition. This results in the increase of the bed armoring effect so that mud resuspension is also significantly restricted.

CONCLUSIONS

A two-dimensional, across-shelf sediment transport model has been developed to simulate storm deposition on continental shelves. The total net seaward sediment transport is small in comparison with the local resuspension and deposition during storms. This is due partly to the poor correlation between the subtidal current and the local wind waves during storms in the study area. The across-shelf variation of storm beds depends on the bottom sediment type. On the sandy inner shelf, the maximum storm-bed thickness is located at the coastal zone and decreases seaward. A small amount of sand is moved seaward even without the littoral sediment input. Storm-bed thickness is increased on the middle and outer shelf because the mud deposits are dominant in these areas. The muddy storm bed has a nearly symmetrical cross-shelf pattern, with a

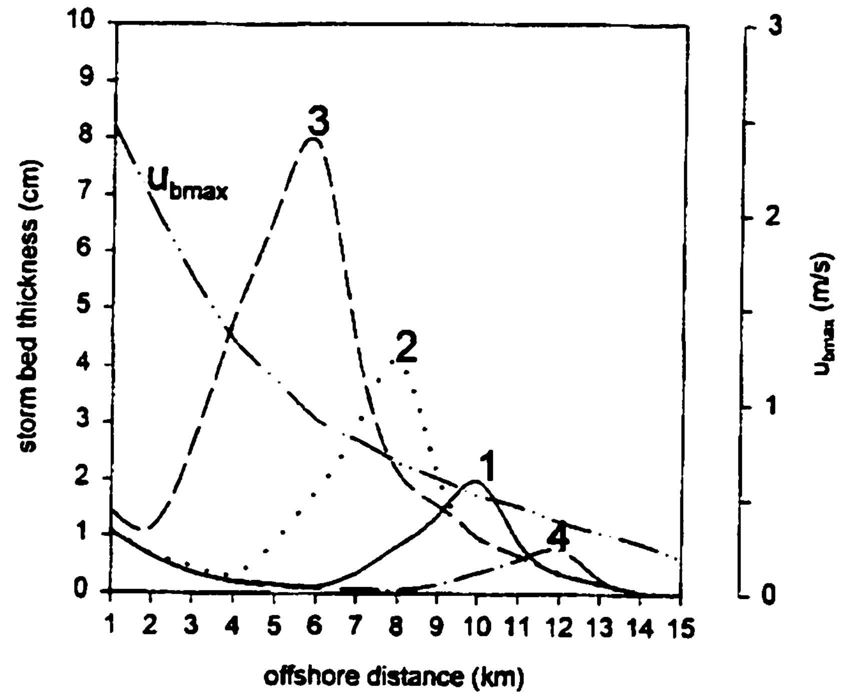

Fig. 23. Across-shelf variation of storm-bed thickness with respect to pre-storm bottom sediment. 1 = present bottom beds at S transect; 2 = mud zone shifts 2 km toward shore; 3 = mud zone shifts 4 km toward shore; 4 = mud zone shifts 2 km toward sea. U_{bmax} is the maximum wave-orbital velocity near bottom.

maximum value at a water depth of about 70 m. This result suggests that the beds found in February of 1995 on the Eel shelf may not have been a direct response to river flooding, but are instead a record of storm-induced resuspension events during a period when flood sediment were available. The Eel River flood sediments found in this new bed appear to have been resuspended, transported and deposited several times by storms and other oceanic force after being discharged from the Eel River. The sensitivity experiments of the model illustrate that the τ_c for mud erosion, and γ_0 for sand are more important than other parameters in determining the storm deposition on the Eel shelf.

CHAPTER IV

SIMULATION OF SEDIMENTARY FACIES ON THE NORTHERN CALIFORNIA SHELF

INTRODUCTION

Facies models for interpretation of sedimentary environments have become increasingly popular among sedimentologists and stratigraphers (Reading, 1986). However, these models are largely descriptive, interpreting sedimentary successions by analogy and pattern-matching techniques. During the same period, there has been intensive study of boundary-layer fluid dynamics and sediment transport on continental shelves, to the point where cross-disciplinary synthesis may lead to important sedimentological insights. To this end, a quantitative, dynamical facies model is developed. The model is used to simulate storm-bed succession on the Eel Shelf, Northern California (Fig. 24). In this chapter, I describe the model and compare the simulations with observations. The hypotheses concerning the facies differentiation are dynamically tested.

Fig. 25 presents a conceptual model for sedimentation and facies development on continental shelves. The conceptual model serves as a framework to which the physics of sediment transport can be attached, for the purposes of modeling. In the conceptual model, a *dispersal system* consists of an assemblage of flow-linked environments characterized by specific dispersal mechanisms (Swift et al., 1991). The nearshore environment is the eroding source environment, whereas successive offshore environments are depositional. The environments create the sedimentary facies that comprise a *depositional system* (an assemblage of process-related facies; Fisher and McGowen, 1967). In a depositional system, facies are systematically arranged along the gradients of sediment grain size and dispersal mechanism and are either stacked on, or are truncated by, a *source diastem*, cut by the shifting source environments (Swift et al., 1991). There have been speculations on the facies differentiation. Russell (1939) explained the horizontal grain-size gradients by a process that he called progressive sorting, in which the coarser particles are preferentially deposited during episodic transport down a dispersal pathway. Crowley (1984) proposed a process of stratal condensation, measured by the ratio of preserved bed thickness to generated bed thickness. Crowley argued that the preservation acts as a low-pass filter to event beds in which the bandwidth of the filter is determined by sedimentation rate. Both of the proposed processes are important for facies differentiation. In this chapter, I test the hypothesis that facies differentiation is controlled by the coupled processes of progressive sorting and stratal condensation through development of a quantitative, dynamical model on the Northern California Shelf.

The Eel River sector of the Northern California Shelf extends for approximately 55 km, and the shelf edge lies at a depth of 100-150 m (Borgeld, 1985). The shoreface is basically an erosional surface, veneered with transient sediment patches that are subject to storm resuspension, and serves as a sediment source (Borgeld, 1985). At large time and space scales, however, the Eel River sector is an accumulation-dominated setting owing to

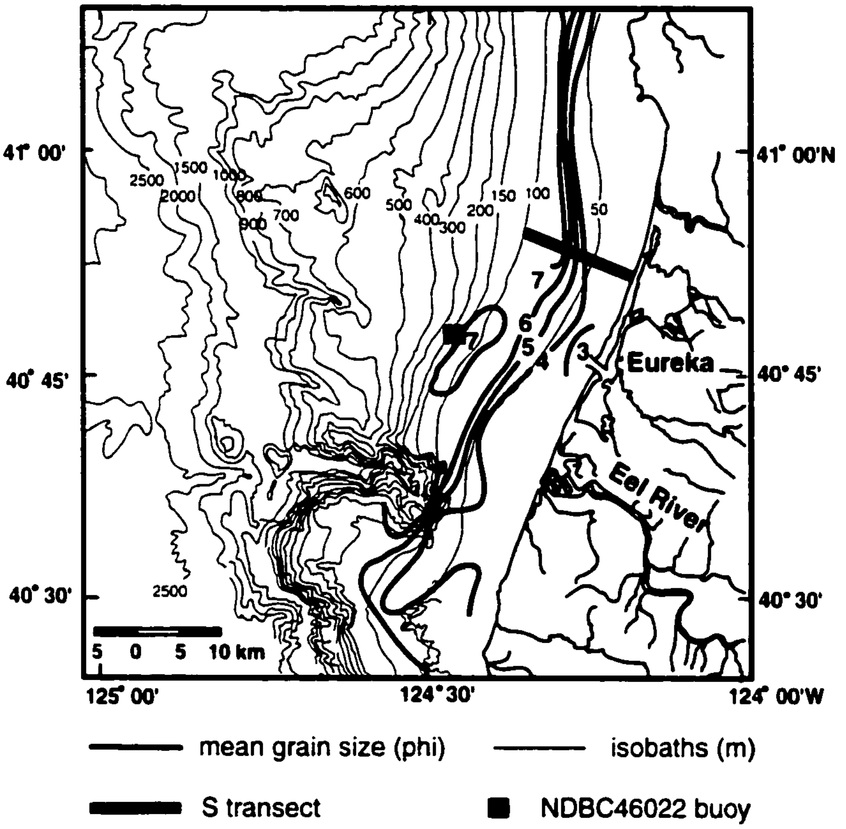
41° 00'
40° 45'
40° 30'
41° 00'N
40° 45'
40° 30'
125° 00'
124° 30'
124° 00'W
2500
1500
1000
2000
800
900
700
600
500
400
300
200
150
100
50
7
6
5
4
3
Eureka
Eel River
2500
5 0 5 10 km
mean grain size (phi)
isobaths (m)
S transect
NDBC46022 buoy

Fig. 24. Eel River sector of the Northern California Shelf, showing grain size gradients (Borgeld, 1985).

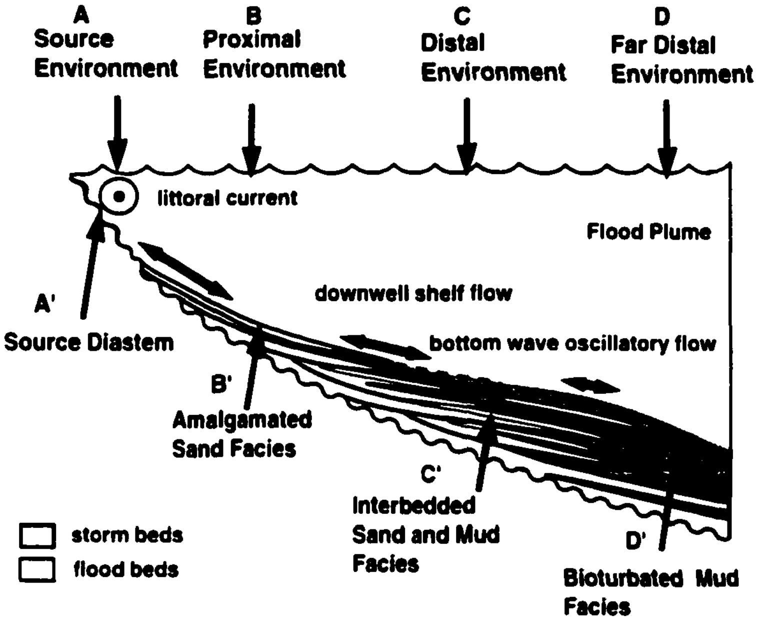
A
Source
Environment
B
Proximal
Environment
C
Distal
Environment
D
Far Distal
Environment
littoral current
Flood Plume
downwell shelf flow
bottom wave oscillatory flow
A'
Source Diastem
B'
Amalgamated
Sand Facies
C'
Interbedded
Sand and Mud
Facies
D'
Bioturbated Mud
Facies
☐ storm beds
☐ flood beds

Fig. 25. Facies template, configured for transgressive shelf setting. 1-4: dispersal mechanisms; A-D: successive environments of dispersal system; A'-D': corresponding facies of the depositional system.

the significant input of muddy fluvial sediments from the Eel and adjacent rivers (Nittrouer and Kravitz, 1995). Flood beds were found in the strata (Borgeld, 1985), but most flood material undergoes storm resuspension.

DYNAMICAL FACIES MODEL

General

The formation of storm-dominated facies can be partitioned into two process-related sedimentation modes, i.e., storm-bed formation and storm-bed succession formation. The former creates individual storm bed at an event scale over a few hours or days duration, whereas the latter produces a bed succession at a facies scale of more than 10^2 years. A storm creates an event bed. Meanwhile, it will simultaneously destroy or modify previously deposited beds. Preservation of a bed with respect to a given subsequent storm depends not only on the intensity of the storm, but also on the extent to which the bed is shielded by the deposits that occurred between the initial storm and the specified later storm. Nevertheless, occurrence of storm is a random process. The proposed facies model is constructed in a coupled numerical-probabilistic approach. A two-dimensional numerical model of cross-shelf sediment transport is developed to simulate storm deposition at an event scale, from which the geometry and sedimentary texture of storm-bed are calculated. Furthermore, a probabilistic model is developed to simulate bed succession (facies) formation by estimating the preservation potential in most likelihood of each storm bed on the basis of the local storm climate.

Storm-Bed Formation

A two-dimensional cross-shelf sediment transport model has been developed to simulate storm deposition on the Eel Shelf, Northern California. The wave height variation during a storm is generalized as a parabolic process with its peak at the middle of the storm duration. Storm sedimentation is decoupled into two basic modes in the model, i.e., a net erosion during the waxing stage of storm and a net deposition during the waning stage of storm. At the waxing period, the bottom boundary of a storm bed corresponds to the maximum erosion depth $E(k)$ on a non uniform sea floor, which is determined by $E(k) = E_s(k) + E_b(k)$, where $E_s(k)$ is the erosion depth caused by resuspension of bottom sediments, $E_b(k)$ is the erosion depth caused by bed load movement, and k is the storm class in terms of return period. Based on the assumption of equilibrium condition during this period, a two-layer, eddy-diffusivity model of the wave-current combined benthic boundary layer, developed by Grant and Madsen (1979) and Glenn and Grant (1987), is used to calculate the time-averaged sediment concentrations in water column. The total volume of sediments that are resuspended into the water column is calculated with respect to the maximum significant wave height of the storm event. Thus, $E_s(k)$ is obtained. A simplified empirical formula, suggested by Nielsen (1992), is used here to calculate the erosion depth, $E_b(k)$, due to bed load transport. If all sediments are not movable during storms, an armored layer will be developed. Under the armoring condition, sediments and flow dynamics cannot reach equilibrium, and the erosion depth $E(k)$ can be calculated from an upper bed layer known as the active layer (Thomas and

Prasuhn, 1977). The expression proposed by Borah et al. (1982) is introduced to calculate the erosion depth under armoring conditions on a well-mixed bed. During the waning stage of storm, a net deposition process occurs because the surface waves are decreasing. A two-dimensional cross-shelf model of suspended sediment transport is used to simulate the net offshore transport and redeposition of storm-induced suspended sediments. The Lagrangian form of the laterally averaged suspended-sediment transport equation (Schoellhamer, 1988) is applied. In this simulation, the net offshore sediment transport occurs within the bottom Ekman layer (Trowbridge et al., 1994), which is poorly related to storm waves in both space and time domains in the study area (Largier et al., 1993). The algorithm described above will produce the maximum erosion depth $E(k)$, the storm-bed thickness $\Delta\eta(k)$, the mean grain size of bed $M_d(k)$, and the net accumulation $A(k) = E(k) - \Delta\eta(k)$, for each class storm.

Storm-bed Succession Formation

Storm sequences are effectively random, so that the time series of storm-bed generated at sea floor is a random process. As a result, storm climate controls the occurrence of storm bed. The probability of occurrence of k class storm bed, therefore, can be described by the *bed generation potential*, $P_g(k)$. This parameter is determined by the probability density function of the local storm climate. As we mentioned previously, the preservation of a storm-bed at sea floor depends on the time series of subsequent storm events. For any storm climate, there are many realizations. Each realization will produce a unique bed succession. It is hard to determine the probability density distribution of storm-bed preservation because the recorded event strata constitute only one sample (realization) in the entire sample space of the storm climate. But the modal realization of this process can be estimated. I propose the *bed preservation potential*, $P_p(k)$, the modal value of storm bed preservation, as a parameter to describe the ratio of preserved thickness to initial thickness of a storm bed. The *conditional preservation potential*, defined as the preservation potential of k class storm bed with respect to the erosion of i class storm, is presented as:

$$P_p(k/i) = \begin{cases} 0 & E(i)-\tilde{A}(i) > \Delta\eta(k) \\ 1-\dfrac{E(i)-\tilde{A}(i)}{\Delta\eta(k)} & \Delta\eta(k) \geq E(i)-\tilde{A}(i) \geq 0 \\ 1 & E(i)-\tilde{A}(i) < 0 \end{cases} \qquad (39)$$

where $\tilde{A}(i)$ is the sum of the sediment accumulations generated by all storms during the return period of i class storm. Obviously, $\tilde{A}(i)$ is a random variable, and it can be estimated by the *bed generation potential* $P_g(k)$,

$$\tilde{A}(i) = N\sum_{j=1}^{i} A(j)P_g(j) \qquad (40)$$

where N is the total number of storms over the time period of concern. As indicated in Eq. 39, the higher the sediment accumulation $\tilde{A}(i)$ is, the higher the preservation potential will be.

The preservation of an initial bed depends on the responses of the bed to all subsequent events. For each k class storm bed, there is a set of *conditional preservation potential*, $\{P_p(k/i)\}$, i varies from 1 to n_k. n_k is the number of storm classes. The final fate of the initial storm bed relies on the minimum conditional preservation potential in this set. Therefore, the bed preservation potential, $P_p(k)$, is defined as

$$P_p(k) = \min \{P_p(k/i)\} \tag{41}$$

The value of $P_p(k)$ varies between 0 to 1. A potential of 1 means that an initial k class storm bed will be totally preserved, and a potential of zero means that this initial k class storm bed will be totally eroded by subsequent storms. A potential between 0 and 1 indicates the fraction of initial storm-bed thickness that survives into permanent burial after erosions of subsequent storms. A modal thickness of k class preserved storm-bed appeared in bed succession is determined by $\Delta\eta(k)*P_p(k)$. By estimating the preservation potentials of all storm-beds, the frequency of the preserved storm-beds and their thickness in a bed succession can be estimated, and the most probable storm-bed succession may thus be predicted.

Model Inputs

A 15 km cross-shelf transect near northern Humboldt Bay (Fig. 24), which extends from the shoreline to a depth of 100 m, has been selected for simulation. The surface grain size distributions used as input for the simulation are derived through averaging and interpolating data from 15 samples collected by Borgeld (1985). The data of Komar and Reimers (1978) are used for sediment settling velocity. The fine silt and clay are assumed to settle as flocs and have an average settling velocity of 0.009 cm/s. The storms are classified by the frequency in terms of return period. The storm climate is described by a Fisher-Tippett distribution (Goda, 1990). Such a distribution, with parameters _ = 0.8 and _ = 5.2 resulting from the best-fitting of NDBC46022 buoy data (Fig. 24), is used to present the local storm climate, from which the storm generation potential $P_g(k)$ is derived.

SIMULATION RESULTS

The simulated initial storm-beds and preserved storm-beds with respect to different storm classes are shown in Fig. 26. The stratal condensation process has left an imprint on the simulated transect. On the Northern California Shelf, the degree of stratal condensation varies with depth and distance from shore. Fig. 26 indicates that in the eroding shoreface environment, all storm beds have a zero preservation potential, which means that any storm-bed will be destroyed by subsequent storms, resulting in a source diastem. Farther offshore, beds from storms of lower frequency but higher power (long-return-period storms) begin to be preserved, but are truncated, while those from storms of higher frequency but lower power (short-return-period storms) are still destroyed. As the water depth increases, the preservation potential increase, leading to the preservation of more and more beds from short-return-period storms in the strata. At outer shelf depths, all storm beds retain their initial thickness.

It has been suggested that the physical preservation process can be viewed as a low-pass filter because the higher-energy, lower-frequency events should dominate the sedimentary record (Crowley, 1984). However, our model shows that the frequency band of this preservation filter varies as a function of position in the dispersal system. The band of the filter extends from the low-frequency end to the high-frequency end as water

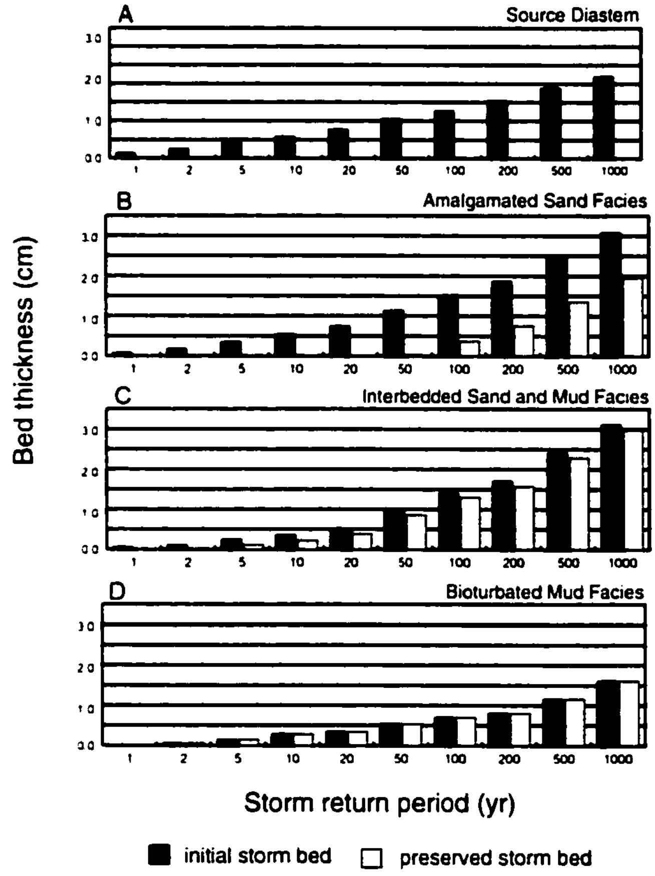

Fig. 26. Degree of stratal condensation for facies on the Northern California Shelf.

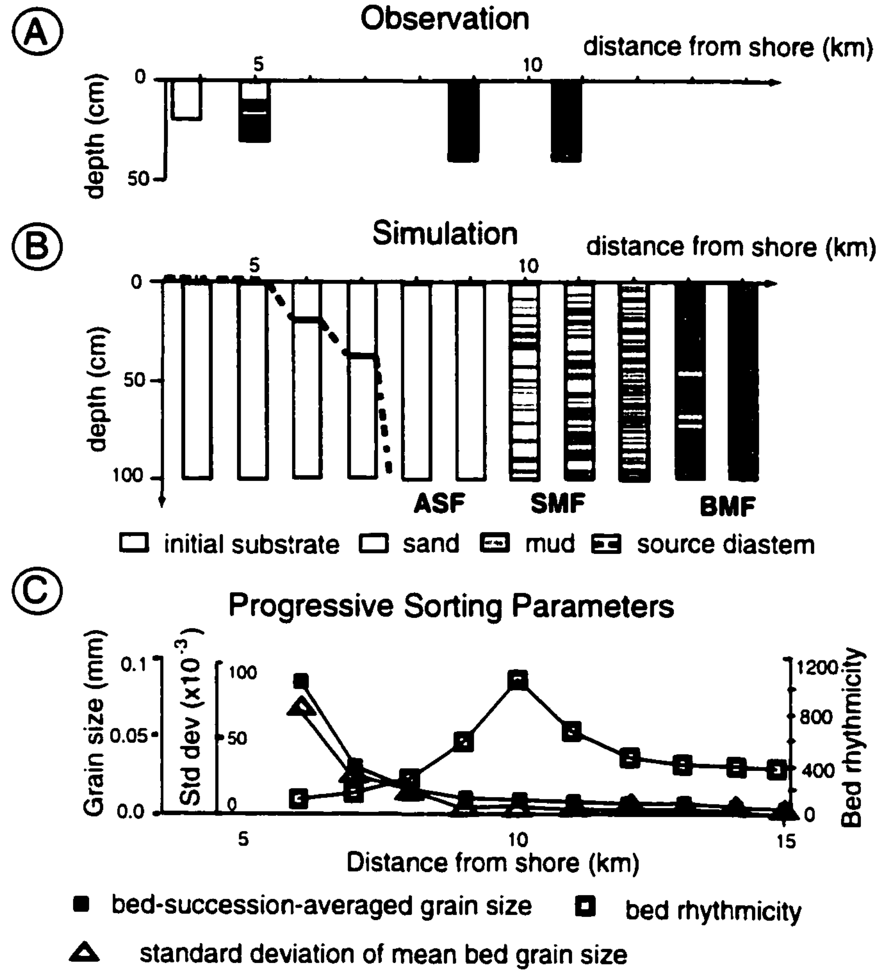

Fig. 27. Simulation vs. observation. A: Box cores (Borgeld, 1985); B: simulation of facies; C: profiles of computed mean, depth averaged grain size and bed rhythmicity (a measure of interbed grain size contrast).

depth increases, contributing significantly to the facies differentiation.

Fig. 27 presents simulated storm-bed successions and compares these successions with box-core data from Borgeld (1985). The three basic facies patterns of a transgressive-shelf depositional system are present. An *amalgamated sand facies* (ASF), is followed seaward by an *interbedded sand and mud facies* (SMF), followed in turn by a *bioturbated mud facies* (BMF). Aspects of the system geometry appear in Fig. 27. The eroding shoreface environment, landward of the several dispersal environments, is undergoing burial and preservation within the evolving depositional system as the source diastem (Swift et al., 1991), or ravinement surface.

The progressive sorting process has left a clear imprint on the simulated transect (Fig. 27C). The bed-succession-averaged grain size and the standard deviation of mean bed grain size exponentially decrease seaward. Bed rhythmicity, defined as the alternativeness of sand bed and mud bed in bed succession, increases seaward with increasing preservation of beds from short-return-period storm, and decreases with decreasing sand deposition.

CONCLUSIONS

A basic problem of geologic modeling has been recognized through the numerical experiments. At short-time scales, the physics of the systems of concern are well understood. For example, a storm bed can be simulated in a deterministic domain for given hydrodynamic and geologic settings. However, at long-time scales, the system responds to random inputs or boundary conditions, for example, storm and flood events. So this system behaves as a stochastic system. Furthermore, the output of this long-term system, i.e., the bed succession, constitutes a biased record that is not consistent with storm and flood histories because of the random preservation process. This problem has been approached by a coupled numerical-probabilistic model. Thus, all processes over different time scales are taken into account. The predictions can be improved by incorporating a river plume model in order to simulate the Eel River flood deposition. Eel River flood climate also needs to be introduced into the calculation of the bed generation potential and the bed preservation potential respectively. The sensitivity experiments of our model demonstrate that the resuspension coefficient, γ_0, is more important than the bottom roughness scaling constant, Ω, in determining the thickness of storm-bed. Decrease of γ_0 leads to decrease of sand deposition, whereas mud deposition is also significantly restricted because of the bed armoring effect.

The resulting computations (Figs. 26 and 27) support the hypothesis that sedimentary facies are produced by the coupled mechanisms of progressive sorting and stratal condensation, in which beds are generated and then modified by successive events as they undergo burial. Further, model results show that the degree of condensation, and the bandwidth and position of the "preservation filter," is a function of the energy gradients of the dispersal system. The model simulations lead to present generalizations concerning the facies formation that I believe to be applicable to a variety of depositional settings. Turbidite, inundite (flood bed), and eolianite successions, like tempestite succession, are event-bed successions generated by random dispersal systems. It is inferred that similar dynamical models can be constructed to describe these depositional settings. Probability frequency distributions of turbidity currents, river floods, and desert dust storms can be evaluated, generation and preservation potentials can be computed, and the facies arrays realized.

BIBLIOGRAPHY

Aigner, T. and Reineck, H.E., 1982. Proximality trends in modern storm sands from the Helegoland Bight (North Sea) and their implications for basin analysis. Senckenbergiana marit. 14, 183-215.

Allen, J.R.L., 1982. Sediment Structures: their character and physical basis. Elsevier, Amsterdam, 664pp.

Ariathurai, R. and Arulanandan, K., 1978. Erosion rate of cohesive soils. J. Hydr. Div. ASCE 104, 279-283.

Ariathurai, R. and Krone, R.B., 1976. Finite element model for cohesive sediment transport. J. Hydrol. Div. ASCE 102, 323-338.

Basco, D.R., 1985. A qualitative description of wave breaking. J. Waterw. Port. Coast. Ocean Eng. ASCE 111, 171-188.

Battjes, J.A. and Janssen, J.P.F.M., 1978. Energy loss and set-up due to breaking of random wave. In: Proc. 16th Coast. Eng. Conf., ASCE, pp569-587.

Battjes, J.A. and Sakai, T., 1981. Velocity field in a steady breaker. J. Fluid Mech. 111, 121-137.

Battjes, J.A., 1974. Surf similarity, In: Proc. 14th Coast. Eng. Conf., ASCE, pp448-480.

Bedford, K.W. and Lee, J., 1994. Near-bottom sediment response to combined wave-current conditions, Mobile Bay, Gulf of Mexico. J. Geophys. Res. 99, 16161-16177.

Berlamont, J., Ockenden, M., Toorman, E. and Winterwerp, J., 1993. The characterization of cohesive sediment properties. Coast. Eng. 21, 105-128.

Bishop, C., Skafel, M. and Nairn, R., 1992. Cohesive profile erosion by waves. In: Proc. 23rd Coast. Eng. Conf., ASCE, pp. 2976-2989.

Borah. D.K., Alonso, C.V. and Prasad, S.N., 1982. Routing graded sediments in streams: formulation. J. Hydraul. Eng. 108, 1486-1503.

Borgeld. J. C., 1985. Holocene stratigraphy and sedimentation on the Northern California continental shelf. Ph.D. Dissertation, Univ. of Washington, 178 pp.

Borgeld, J.C., Hughes Clarke, J.E., Goff, J.A., Mayer, L.A. and Curtis, J.A., 1999. Acoustic backscatter of the 1995 flood deposit on the Eel River shelf. Mar. Geol. 154, 197-210.

Burban, P.Y., Xu, Y.J., McNell, J. and Lick, W., 1990. Settling speeds of flocs in fresh water and seawater. J. Geophys. Res. 95, 18213-18220.

Cacchione, D.A. and Drake, D.E., 1982. Measurements of storm-generated bottom stresses on the continental shelf. J. Geophys. Res. 87, 1952-1960.

Cacchione, D.A., Grand, W.D., Drake, D.E. and Glenn, S.M., 1987. Storm-dominated bottom boundary layer dynamics on the California continental shelf: measurements and predictions. J. Geophys. Res. 92, 1817-1827.

Cacchione, D.A., P.L. Wiberg, P.L., Lynch, J., Irish, L., and Traykovski, P.A., 1999. Estimates of suspended sediment flux and bedform activity on the inner portion of the Eel continental shelf. Mar. Geol. 154, 83-97.

Camerlengo, A.L. and O'Brien, J.J., 1980. Open boundary conditions in rotating fluids. J. Comp. Phys. 35, 12-35.

Carey, J.S., Swift, D.J.P., Steckler, M., Reed, C.W., and Niedoroda, A.W., 1999. High resolution sequence stratigraphy modeling: effects of sedimentation processes in numerical experiments in stratigraphy. Soc. Econ. Paleontol. Mineral. Spec. Publ., 151-164.

Chorley, R.J., Schumm, S.A. and Sugden, D.E., 1984. Geomorphology. Methuen, 605pp.

Coleman, J.M., 1988. Dynamic changes and processes in the Mississippi River delta. Geol. Soc. Amer. Bull. 100, 999-1015.

Cox, D.T., Kobayashi, N. and Okayasu, A., 1996. Bottom shear stress in the surf zone. J. Geophys. Res. 101, 14337-14348.

Crowley, K.D., 1984. Filtering of depositional events and the completeness of sedimentary sequences. J. Sed. Petrol. 54, 127-136.

Curray, J.R., 1960. Sediments and history of the Holocene transgression, continental shelf, northwest Gulf of Mexico. In: Shepard, F.P., Phleger, F.B. and Van Andel, T.H. (Eds.), Recent Sediments, northwest Gulf of Mexico, Amer. Assoc. Petrol. Geol., pp. 221-226.

Curray, J.R., 1964. Transgressions and regressions. In: Miller, R.L. (Ed.), Papers in Marine Geology. Shepard commemorative volume, MacMillan, New York, pp. 175-203.

Curray, J.R., 1969. Shore zone sand bodies: barriers, cheniers, and beach ridges. In: Stanley, D.J. (Ed.), The New Concepts of Continental Margin Sedimentation. AGI, Washington, D.C., JCII-1-18.

Davidson-Arnott, R.G.D., 1986. Rates of erosion of till in the nearshore zone. Earth Surf. Proc. Landforms 11, 53-58.

Davidson-Arnott, R.G.D. and Ollerhead, J., 1995. Nearshore erosion on a cohesive shoreline. Mar. Geol. 122, 349-365.

Dean, R.G., 1991. Equilibrium beach profiles: Characteristics and applications. J. Coast. Res. 7, 53-84.

Deigaard, R., Fredsoe, J. and Hedegaard, I.B., 1986. Suspended sediment in the surf zone. J. Waterw. Port, Coast. Ocean Eng. 112, 115-128.

DeVries, J.W., 1992. Field measurements of the erosion of cohesive sediments. J. Coast. Res. 8, 312-318.

Dietz, R.S., 1963. Wave base, marine profile of equilibrium, and wave built terraces: a critical appraisal. Geol. Soc. Amer. Bull. 74, 971-990.

Duke, W.L., Arnott, R.W. and Cheel, R.J., 1991. Shelf sandstones and hummocky cross stratification: new insights on a stormy debate. Geology 19, 625-628.

Dyer, K.R. and Soulsby, R.L., 1988. Sand transport on the continental shelf. Annual Rev. Fluid Mech. 20, 295-324.

Eidsvik, K.J., 1993. Parameterization of wave effects upon large-scale bottom boundary layer flow. Cont. Shelf Res. 13, 903-918.

Emery, K.O., 1952. Continental shelf sediments off southern California. Geol. Soc. Amer. Bull. 63, 1105-1108.

Fenneman, N.M., 1902. Development of the profile of equilibrium of the subaqueous shore terrace. J. Geol. 10, 1-32.

Fisher, W.L., and McGowen, J.H., 1967. Depositional systems in the Wilcox Group of Texas and their relationship to the occurrence of oil and gas. Gulf Coast Assoc. Geol. Soc. Trans. 17, 105-125.

Fredericks, J.J., Trowbridge J.H., Williams III, A.J., Lentz, S.J., Butman, B. and Gross, T.F., 1993. Fluid mechanical measurements within the bottom boundary layer over the northern California continental shelf during STRESS. Technical Report, WHOI-93-32, Woods Hole Oceanography Institution, 116pp.

Fredsoe, J. and Deigaard, R., 1992. Mechanics of Coastal Sediment Transport. World Scientific, 369pp.

Glenn, S.M., and Grant, W.D., 1987. A suspended sediment stratification correction for combined wave and current flows. J. Geophys. Res. 92, 8244-8264.

Goda, Y., 1990. Distribution of sea state parameters and data fitting. In: Herbich, J.B., (Ed.), Handbook of coastal and ocean engineering, Vol.1. Gulf Publishing Company, Houston, pp. 371-408.

Grant, W.D. and Madsen, O.S., 1979. Combined wave and current interaction with a rough bottom. J. Geophys. Res. 84, 1797-1808.

Grant, W.D. and Madsen, O.S., 1986. The continental-shelf bottom boundary layer. Ann. Rev. Fluid Mech. 18, 265-305.

Green, M.O., Vincent, C.E., McCave, I.N., Dickson, R.R., Rees, J.M. and Pearson, N.D., 1995. Storm sediment transport: observations from the British North Sea shelf. Cont. Shelf Res. 15, 889-912.

Gross, T.F., Isley, A.E. and Sherwood, C.R., 1992. Estimation of stress and bed roughness during storms on the Northern California shelf. Cont. Shelf Res. 12, 389-413.

Gu, J.L., Gong, C.Z. and Lu, X.L., 1990. The threshold movement of cohesive sediment due to wave action (in Chinese). In: Gong, C.Z. (Ed.), Sediment Deposition in Lianyungang. Hehai University Press, Nanjing, pp. 116-124.

Horn, D.P., 1992. A review and experimental assessment of equilibrium grain size and the ideal wave-graded profile. Mar. Geol. 108, 161-174.

Huang, J.W. and Sun, X.Q., 1985. Experiments on erosion of sediments in Lianyungang (in chinese). Rept. of Nanjing Hydralic. Research. Inst., 17pp.

Hughes, S.A. and Miller, H.C., 1987. Transformation of significant wave height. J. Waterw. Port Coast. Ocean Eng. ASCE 113, 588-605.

Jin, L. and Zhang, Q.S., 1983. Estimation of elements of design waves in Lianyungang (in Chinese). In: Proc. of Conf. on Wind Waves in Lianyungang, Jiangsu.

Johnson, D.W., 1919. Shore Processes and Shoreline Development. John Wiley, New York, 584pp.

Jonsson, I.G., 1966. Wave boundary layers and friction factors. In: Proc. 10th Coast. Engr. Conf., ASCE, pp. 127-148.

Kamphuis, J.W., 1987. Recession rate of glacial till bluffs. J. Waterw. Port, Coast. Ocean Eng. ASCE 113, 60-73.

Kamphuis, J.W., 1990. Influence of sand and gravel on the erosion of cohesive sediment. J. Hydr. Res. 28, 43-53.

Komar, P.D., and Reimers, C.E., 1978. Grain shape effects on settling rates. J. Geol. 86, 193-209.

Krone, R.B., 1962. Flume studies of the transport of sediment in estuarial shoaling processes. Final Report, Hydr. Engr. Lab. and Sanitary Engr. Res. Lab., U. of California, Berkeley, 110 pp.

Kulm, L.D., Roush, R.C., Harlett, J.D., Neudeck, R.H., Chambers, D.M. and Runge, E.J., 1975. Oregon continental shelf sedimentation: interrelationships of facies distribution and sedimentary processes. J. Geol. 83, 145-176.

Largier, J.L., Magnell, B.A., and Winant, C.D., 1993. Subtidal circulation over the Northern California shelf. J. Geophys. Res. 98, 18147-18179.

Lippmann, T.C., Brookins, A.H. and Thornton, E.B., 1996. Wave energy transformation on natural profiles. Coast. Eng. 27, 1-20.

Lyne, V.D., Butman, B. and Grant, W.D., 1990. Sediment movement along the U.S. east coast continental shelf, II: Modeling suspended sediment concentrations and transport rates during storms. Cont. Shelf Res. 10, 429-460.

Madsen, O.S., Wright, L.D., Boon, J.D. and Chisholm, T.A., 1993. Wind stress, bed roughness and sediment suspension on the inner shelf during an extreme storm event. Cont. Shelf Res. 13, 1303-1324.

Mehta, A.J., Hayter, E.J., Parker, W.R., Krone, R.B. and Teeter, A.M., 1989. Cohesive sediment transport, I: Process description. J. Hydra. Engr. 115, 1076-1093.

Migniot, C., 1968. A study of the physical properties of different very fine sediments and their behavior under hydrodynamic action(in French). La Houille Blanche 7, 591-620.

Mimura, N., 1993. Rates of erosion and deposition of cohesive sediments under wave action. In: Mehta, A.J. (Ed.), Nearshore and Estuarine Cohesive Sediment Transport, AGU, pp. 247-264.

Moore, D.G. and Curray, J.R., 1964. Wave base, marine profile of equilibrium and wave built terraces, discussion. Geol. Soc. Amer. Bull. 47, 1267-1274.

Nairn, R.B. and Southgate, H.N., 1993. Deterministic profile modeling of nearshore processes, Part II: Sediment transport and beach profile development. Coast. Eng. 19, 57-96.

Nicholson, J. and O'Connor, B.A., 1986. Cohesive sediment transport model. J. Hydr. Eng. ASCE 112, 621-640.

Niedoroda, A.W., Swift, D.J.P. and Thorne, J.A., 1989. Modeling shelf storm beds: Controls of bed thickness and bedding sequence. In: R.A. Morton and D. Nummedal (Eds.), Shelf Sedimentation, Shelf Sequence and Related Hydrocarbon Accumulation, Gulf Coast Section, 7th Annu. Res. Conf. Proc., SEPM, pp. 15-39.

Niedoroda, A.W., Reed, C.W., Swift, D.J.P., Arato, A. and Hoyanagi, K., 1995. Modeling shore-normal large scale coastal evolution. Mar. Geol. 126, 180-200.

Nielsen, P., 1981. Dynamics and geometry of wave-generated ripples. J. Geophys. Res. 86, 6467-6472.

Nielsen, P., 1992. Coastal bottom boundary layers and sediment transport. World Scientific Publishing Company, Singapore, 324 pp.

Nittrouer, C.A. and Sternberg, R.W., 1981. The formation of sedimentary strata in an allochthonous shelf environment: the Washington Continental Shelf. Mar. Geol. 42, 201-232.

Nittrouer, C.A. and Wright, L.D., 1994. Transport of particles across continental shelves. Rew. Geophys. 32, 85-113.

Nittrouer, C.A., and Kravitz, J.H., 1995. Integrated continental margin research to benefit earth and ocean sciences. Eos, Trans. AGU 76, 121-126.

Odd, N.V.M. and Owen, M.W., 1972. A two-layer model of mud transport in the Thames Estuary. Proc. Inst. Civ. Engs., Suppl. 9, 175-205.

Parchure, T.M. and Mehta. A.J., 1985. Erosion of soft cohesive sediment deposits, J. Hydr. Eng. ASCE 111, 1308-1326.

Partheniades, E., 1965. Erosion and deposition of cohesive soils. J. Hydra. Div. ASCE 91, 105-139.

Partheniades, E., 1986. A fundamental framework for cohesive sediment dynamics. In: Mehta, A.J. (Ed.), Estuarine Cohesive Sediment Dynamics. Springer, Berlin, pp. 219-250.

Partheniades, E., 1993. Turbulence, flocculation and cohesive sediment dynamics. In: Mehta, A.J. (Ed.), Nearshore and Estuarine Cohesive Sediment Transport. AGU, Washington, D.C., pp. 40-59.

Peregrine, D.H. and Svendsen, I.A., 1978. Spilling breaker, bores and hydraulic jumps. In: Proc. 16th Coast. Engr. Conf., ASCE, pp. 540-550.

Pilkey, O.H., Young, R.S., Riggs, S.R., Smith, A.W.S., Wu, H. and Pilkey, W.D., 1993. The concept of shoreface profile of equilibrium: A critical review. J. Coast. Res. 9, 255-278.

Qian, N. and Dai, D.Z., 1980. The problems of river sedimentation and the present status of its research in China. In: Proc. Int. Symp. River Sed. pp. 1-39.

Reading, H. C., 1986. Sedimentary environment and facies. Blackwell Scientific Publications, Oxford, 615 pp.

Reed, C.W., Niedoroda, A.W. and Swift, D.J.P., 1999. Modeling sediment entrainment and transport processes limited by bed armoring. Mar. Geol. 154, 143-154.

Rhodes, E.G., 1982. Depositional model for a Chenier Plain, Gulf of Carpenteria, Australia. Sedimentology 29, 201-221.

Roed, L.P. and Smedstad, O.M., 1984. Open boundary conditions for forced waves in a rotating fluid. J. Sci. Stat. Comp. 5, 414-426.

Roelvink, J.A. and Broker, I., 1993. Cross-shore profile models. Coast. Eng. 21, 163-191.

Russell, R.D., 1939. Effects of transportation on sedimentary particles. In: Trask, P.D. (Ed.)., Recent Marine Sediments. Amer. Assoc. Petrol. Geol., pp. 32-47.

Sallenger, Jr., A.H. and Holman, R.A., 1985. Wave energy saturation on a natural beach of variable slope. J. Geophys. Res. 90, 11939-11944.

Schoellhamer, D.H., 1988. Two-dimensional Lagrangian simulation of suspended sediment. J. Hydr. Eng. 114, 1192-1209.

Schunemann, M. and Kuhl, H., 1993. Experimental investigations of the erosional behavior of naturally formed mud from the Elbe estuary and adjacent Wadden Sea, Germany. In: Mehta, A.J. (Ed.), Nearshore and Estuarine Cohesive Sediment Transport. AGU, Washington, D.C., pp. 314-330.

Seilacher, A., 1982. General remarks about event deposits. In: Einsele, G. and Seilacher, A. (Eds.), Cyclic and Event Stratification. Springer-Verlag, pp. 161-174.

Shepard, F.G., 1932. Sediments on continental shelves. Geol. Soc. Amer. Bull. 43, 1017-1039.

Sherwood, C.R., Butman, B., Cacchione, D.A., Drake, D.E., Gross, T.F., Sternberg, R.W., Wiberg, P.L. and Williams III, A.J., 1994. Sediment-transport events on the northern California continental shelf during the 1990-1991 STRESS experiment. Cont. Shelf Res. 14, 1063-1099.

Shi, N., Larsen, L.H. and Downing, J.P., 1985. Predicting suspended sediment concentration on continental shelves. Mar. Geol. 62, 255-275.

Skafel, M.G. and Bishop, C.T., 1994. Flume experiments on the erosion of till shores by waves. Coast. Eng. 23, 329-348.

Sleath, J.F.A., 1991. Velocities and shear stresses in wave-current flows. J. Geophys. Res. 96, 15,237-15,244.

Smith, J.D. and McLean, S.R., 1977. Boundary layer adjustments to bottom topography and suspended sediment. In: J.C.J. Nihoul, J.C.J. (Ed.), Bottom Turbulence. Elsevier, Amsterdam, pp. 1213-1250.

Sternberg, R.W., Ogston, A. and Johnson, R., 1996. A video system for in situ measurement of size and settling velocity of suspended particulates. J. Sea Res. 36, 127-130.

Svendsen, I.A., 1987. Analysis of surf zone turbulence. J. Geophys. Res. 92, 5115-5124.

Swart, D. H., 1974. Offshore sediment transport and equilibrium beach profiles. Delft. Hydr. Lab. Publ., No.131, 32 pp.

Swift, D.J.P., 1970. Quaternary shelves and the return to grade. Mar. Geol. 8, 5-30.

Swift, D.J.P., Ludwick, J.C. and Boehmer, W.R., 1972. Shelf sediment transport, a probability model. In: Swift, D.J.P., Duane, D.B. and Pilkey, O.H. (Eds.), Shelf Sediment Transport: Process and Pattern. Dowden Hutchinson & Ross, Stroudsburg, PA, pp. 195-223.

Swift, D.J.P., 1974. Continental shelf sedimentation. In: Burk, C.A. and Drake, C.L. (Eds.), The Geology of Continental Margins. Springer-Verlag, New York, pp. 117-135.

Swift, D.J.P., Sears, P.C., Bohlke, B. and Hunt, R., 1978. Evolution of a shoal retreat massif, North Carolina shelf: inferences from area geology. Mar. Geol. 27, 19-42.

Swift, D.J.P. and Field. M.E., 1981. Evolution of a classic sand ridge field: Maryland sector, North America inner shelf. Sedimentology 28, 461-482.

Swift, D.J.P., Han, G. and Vincent, C.E., 1986. Fluid process and sea floor response on a modern storm-dominated shelf: middle Atlantic shelf of North America, Part I: the storm current regime. In: Knight, R.L. and McLean, J.R. (Eds.), Shelf Sands and Sandstone Reservoirs. Can. Soc. Petrol. Geol. Mem. 11, pp. 99-119.

Swift, D.J.P., Phillips, S. and Thorne, J.A., 1991. Sedimentation on continental margins, IV: lithofacies and depositional systems. Spec. Publ. Int. Ass. Sediment. 14, 89-152.

Teisson, C., Ockenden, M., Le Hir, P., Kranenburg, C. and Hamm, L., 1993. Cohesive sediment transport processes. Coast. Eng. 21, 129-162.

Thomas, W.A. and Prasuhn, A.L., 1977. Mathematical modeling of scour and deposition. J. Hydra. Eng. 103, 851-863.

Thorne, J.A., Grace, E., Swift, D.J.P. and Niedoroda, A.W., 1991. Sedimentation on continental margins, III: the depositional fabric - an analytical approach to stratification and facies identification. Spec. Publ. Int. Ass. Sediment. 14, 59-87.

Thornton, E.B. and Guza, R.T., 1982. Transformation of wave height distribution. J. Geophys. Res. 88, 5925-5938.

Ting, C.K.F. and Kirby, J.T., 1996. Dynamics of surf-zone turbulence in a spilling breaker. Coast. Eng. 27, 131-160.

Trowbridge, J.H., Butman, B., and Limeburner, R., 1994. Characteristics of the near-bottom suspended sediment field over the continental shelf off northern California based on optical attenuation measurements during STRESS and SMILE. Cont. Shelf Res. 14, 1257-1272.

Tucker, M.J., 1991. Waves in Ocean Engineering. Ellis Horwood Ltd., 431pp.

Van Leussen, W., 1988. Aggregation of particles, settling velocity of mud flocs - a review. In: Dronkers, J. and van Leussen, W. (Eds.), Physical Processes in Estuaries. Springer Verlag, Berlin, pp. 347-403.

Walker, R.C. and James, N.P., 1992. Facies Models: Response to sea level change. Geol. Assoc. Can., 454pp.

Wells, J.T. and Coleman, J.M., 1981. Physical processes and fine-grained sediment dynamics, coast of Surinam, South America. J. Sed. Petrol. 51, 1053-1068.

Wheatcroft, R.A., Borgeld, J.C., Born, R.S., Drake, D.E., Leithold, E.L., Nittrouer, C.A. and Sommerfield, C.K., 1996. The anatomy of an oceanic flood deposit. Oceanography. 8, 158-162.

Wheatcroft, R.A., Sommerfield, C.K., Drake, D.E., Borgeld, J.C. and Nittrouer, C.A., 1997. Rapid and widespread dispersal of flood sediment on the northern California margin. Geology 25, 163-166.

Wiberg, P.L., Drake, D.E. and Cacchione, D.A., 1994. Sediment resuspension and bed armoring during high bottom stress events on the northern California inner continental shelf: Measurements and predictions. Cont. Shelf Res. 14, 1191-1219.

Wright, L.D., Boon, J.D., Green, M.O. and List, J.H., 1986. Response of the mid shoreface of the southern mid-Atlantic Bight to a "northeaster". Geo-Mar. Letters. 6, 153-160.

Wright, L.D., Boon, J.D., Kim, S.C. and List, J.H., 1991. Modes of cross-shore sediment transport on the shoreface of the Middle Atlantic Bight. Mar. Geol. 96, 19-51.

Wright, L.D., Xu, J.P. and Madsen, O.S., 1994. Across-shelf benthic transports on the inner shelf of the Middle Atlantic Bight during the "Halloween Storm" of 1991. Mar. Geol. 118, 61-77.

Wright, L.D., Kim, S.C. and Friedrichs, C.T., 1999. Across-shelf variations in bed roughness, bed stress and sediment suspension on the northern California shelf. Mar. Geol. 154, 99-115.

Xu, J.P. and Wright, L.D., 1995. Tests of bed roughness models using field data from the Middle Atlantic Bight. Cont. Shelf Res. 15, 1409-1434.

You, Z.J., 1994. A simple model for current velocity profiles in combined wave-current flows. Coast. Eng. 23, 289-304.

Yu, Z.Y., Zhang, Y., Chen, D.C. and Jin, L., 1987. The hydrodynamic characteristics of nearshore waters and the discharging process on mud flats. Chin. J. Oceanol. Limnol. 5, 95-106.

Yu, Z.Y., Chen, D.C., Tang, Y.D., Jin, L. and Hao, X.J., 1990. The analysis of the problems concerning the building of Lianyungang deep-water outer navigation channel (in Chinese). In: Gong, C.Z. (Ed.), Sediment Deposition in Lianyungang. Hehai University Press, pp. 202-213.

Zhang, Y., Yu, Z.Y. and Jin, L., 1989. Suspended sediment regression model on mud coasts. In: S.Y. Wang, S.Y.(Ed.), Proc. Int. Symp. Sed. Trans. Model, ASCE, pp. 486-491.

Zhang, Y., Swift, D.J.P., Niedoroda, A.W., Reed, C.W. and Thorne, J.A., 1997. Simulation of sedimentary facies on the Northern California Shelf. Geology 25, 635-638.

Zhang, Y., Swift, D.J.P., Yu, Z., and Jin, L., 1998. Modeling of coastal profile evolution on the abandoned delta of the Huanghe River. Mar. Geol. 145, 133-148.

Zhang, Y., Swift, D.J.P., Fan, S., Niedoroda, A.W., Reed, C.W., 1999. Two-dimensional numerical modeling of storm deosition on the northern California shelf. Mar. Geol. 154, 155-167.

VITA

YONG ZHANG

Department of Ocean, Earth & Atmospheric Sciences
Old Dominion University
4600 Elkhorn Avenue, Norfolk, VA 23529-0276

Date of birth: August 9, 1956
Place of birth: Shanghai, China

EDUCATION

2001 Doctor of Philosophy in Oceanography
Department of Ocean, Earth & Atmospheric Sciences
Old Dominion University
4600 Elkhorn Avenue
Norfolk, VA 23529-0276

1984 Master of Science in Physical Geography
Institute of Estuarine and Coastal Research
East China Normal University
North Zhongshan Rd. 3663
Shanghai, 200062 China

1982 Bachelor of Science in Geography
Department of Geography
East China Normal University
North Zhongshan Rd. 3663
Shanghai, 200062 China